

# Short-period Post-Common Envelope Binaries with Balmer Emission from SDSS and LAMOST Based on ZTF Photometric Data

Li Lifang,<sup>1,2,3\*</sup> and Zhang Fenghui,<sup>1,2,3</sup>

<sup>1</sup>Yunnan Observatories, Chinese Academy of Sciences, 650216, Kunming, P.R. China

<sup>2</sup>Center for Astronomical Mega-Science, Chinese Academy of Sciences, 20A Datun Road, Beijing, 100012, P.R. China

<sup>3</sup>Key Laboratory for the Structure and Evolution of Celestial Objects, Chinese Academy of Sciences, 650216, Kunming, P.R. China

Accepted yymmdd. Received yymmdd; in original form yymmdd

## ABSTRACT

We present here 55 short period PCEBs containing a hot WD and a low-mass MS. Based on the photometric data from ZTF DR19, the light curves are analyzed for about 200 WDMS binaries with emission line(s) identified from SDSS or LAMOST spectra, in which 55 WDMS binaries are found to exhibit variability in their luminosities with a short period and are thus short-period binaries (i.e. PCEBs). In addition, it is found that the orbital periods of these PCEBs locate in a range from 2.2643 to 81.1526 hours. However, only 6 short-period PCEBs are newly discovered and the orbital periods of 19 PCEBs are improved in this work. Meanwhile, it is found that three objects are newly discovered eclipsing PCEBs, and a object (i.e. SDSS J1541) might be the short-period PCEB with a late M-type star or a brown dwarf companion based on the analysis of its spectral energy distribution. At last, the mechanism(s) being responsible for the emission features in the spectra of these PCEBs are discussed, the emission features arising in their optical spectra might be caused by the stellar activity or an irradiated component owing to a hot white dwarf companion because most of them contain a white dwarf with an effective temperature higher than  $\sim 10,000$  K.

**Key words:** stars:binaries (including multiple); close – Stars: AGB and post-AGB – Stars: white dwarfs – Stars: evolution

## 1 INTRODUCTION

The typical final products of stellar evolution for about 98 per cent of main sequence (MS) stars are white dwarfs (WDs), because their masses are too lower to ignite He, C / O, or ONe so that nuclear reactions ceases, leaving a degenerate core of He, C / O, or ONe after their envelopes are lost owing to stellar wind or mass transfer interactions (Brown et al. 2011; Gil-Pons & García-Berro 2001). However, in some cases, He is ignited if no mass transfer interactions take place or they take place in AGB. Meanwhile, He in the core is also probably ignited if the rapid mass transfer interactions take place near the tip of RGB then leave a hot subdwarf ( $\sim 0.5M_{\odot}$ ) with a shell mass of  $\lesssim 0.02M_{\odot}$  (Heber 1986; Han et al. 2002; Lei et al. 2013). Close compact binaries are usually thought to be the products of common envelope (CE) evolution (Paczýński 1976) which is a result of the unstable mass transfer depended on the mass ratio of binary systems (Nebot Gómez-Morán et al. 2011; Rappaport et al. 2017) once the massive star is on the giant branch (GB) or asymptotic giant branch (AGB) with a radius of about  $100 R_{\odot}$  (Webbink 1984; Willems & Kolb 2004) and about 25 per cent binaries would undergo CE phase (Willems & Kolb 2004; Parsons et al. 2017). During the CE phase, the orbital energy of the donor’s core and its companion is rapidly injected into the CE owing to differential rotation, decreasing the separation between two components of binary system. If the orbital energy is enough to eject the envelope before merger, exposing a post-common envelope binary (PCEB), consisting of a WD and a

companion, generally an MS star (Webbink 1984; Kao et al. 2016; Rappaport et al. 2017).

The CE evolution phase plays an important role in many evolutionary pathways leading to the formation of compact objects in short period binaries, such as millisecond pulsars, X-ray binaries, CVs, double WDs, double neutron stars, and strongly magnetized WDs, or even double black holes (Taam & Sandquist 2000; Nebot Gómez-Morán et al. 2009; Rebassa-Mansergas et al. 2007, 2012; Nordhaus 2011; Abbott et al. 2016). Although the main features in CE phase had been sketched by Paczýński (1976) more than 40 years ago, then a lot of studies on the formation of PCEBs had been carried out by many investigators (e.g. Webbink 1984; Iben & Livio 1993; Willems & Kolb 2004; Davis et al. 2008; Politano et al. 2010), our understanding on the CE evolution is still very poor (Politano & Weiler 2007; Nebot Gómez-Morán et al. 2009; Rebassa-Mansergas et al. 2012). Any significant progress in our understanding of the CE evolution certainly requires both unrelenting theoretical efforts and innovative observational input (Schreiber et al. 2008). Since the CE phase usually lasts a very short timescale ( $\lesssim 1000$  yrs, Hjellming & Taam 1991; Taam & Sandquist 2000; Webbink 2008) and is thus virtually impossible to observe directly. The heavy responsibility of restricting the CE phase falls on objects that have most probably undergone a CE phase in their past (van den Besselaar et al. 2007). Among all PCEBs, those containing a WD and a MS star, i.e. WDMS binaries, represent the most promising population for deriving such observational constraints since they are very common population of PCEBs (Nebot Gómez-Morán et al. 2009, 2011; Rebassa-Mansergas et al. 2012).

Up to now, about 5,000 WDMS binaries have been discovered by

\* E-mail: llf@ynao.ac.cn or Zhangfh@ynao.ac.cn

various investigators (Silvestri et al. 2006; Heller et al. 2009; Liu et al. 2012; Rebassa-Mansergas et al. 2013a; Ren et al. 2013; Li et al. 2014; Guo et al. 2015) based on SDSS (York et al. 2000) or LAMOST spectra since Raymond et al. (2003) and Schreiber & Gänsicke (2003) first attempted to study the WDMS binaries in SDSS. Meanwhile, near 600 WDMS binaries had been identified based on the location within the H-R diagram based on Gaia photometric magnitudes (Rebassa-Mansergas et al. 2021, 2023). However, the orbital periods of only a small portion of them had been determined by various investigators through radial velocity observations (e.g. Rebassa-Mansergas et al. 2008; Pyrzas et al. 2009; Nebot Gómez-Morán et al. 2011; Parsons et al. 2021) or photometric data of CRTS, PTF or ZTF (e.g. Parsons et al. 2013; Drake et al. 2014; Parsons et al. 2015, 2017; Chen et al. 2020; Brown et al. 2022) although the number of WDMS binaries with determined orbital periods is gradually increasing. In the discovered PCEBs, some of them were found to contain a low mass He WD and a MS companion with  $M \lesssim 0.2M_{\odot}$  (Nebot Gómez-Morán et al. 2011; Luhman et al. 2011; Xu et al. 2015; Farihi et al. 2017; Rappaport et al. 2017), however the oldest globular clusters in the Galactic halo are currently producing  $\sim 0.53M_{\odot}$  WDs from MS progenitors with  $M \lesssim 0.8M_{\odot}$  (Kalirai et al. 2009; Brown et al. 2011; Rebassa-Mansergas et al. 2011). Therefore, the low-mass He WDs in these binaries should be formed from the enhanced mass loss from post-MS stars without reaching asymptotic branch (AGB) and without ever igniting He in interacting binaries (Webbink 1984; Nebot Gómez-Morán et al. 2009; Brown et al. 2011). Although the formation scenario for such binaries had been proposed by Nelemans & Tauris (1998), however, we do not know how is the relatively dense envelope of their progenitors with mass more than  $1.0 M_{\odot}$  expelled by a low-mass companion with a relatively low orbital energy. In fact, there are a fair number of single low-mass WDs that show neither variability in their radial velocities nor infrared excess (Rebassa-Mansergas et al. 2013a). The existence of single low-mass WDs had been explained by many investigators (e.g. Han et al. 2002; Killic, Stanek & Pinsonneault 2007; Justham et al. 2009). Therefore, it is necessary to find more PCEBs for limiting the results of CE evolution.

In this work, the light curves from ZTF DR19 are analyzed for about 200 WDMS binaries with emission lines identified from SDSS or LAMOST, then 55 WDMS binaries are found to be PCEBs with a short period located in a range from 2.2643 to 81.1526 hours. Among these PCEBs, only 6 are newly discovered, and the orbital periods of 19 PCEBs are improved. In addition, three new eclipsing PCEBs are found out from these PCEBs based on their light curves. The analysis of the photometric data collected from ZTF survey is presented in Sect. 2. In Sect. 3, we discuss the results and draw our conclusions,

## 2 PHOTOMETRIC DATA ANALYSIS

Although many WDMS binaries (about 6,000) were identified based on their spectra from SDSS and LAMOST or by their location in H-R diagram based on the Gaia photometric observations, however only a small portion of them were found to be the short-period PCEBs through the analysis of their radial velocities or light curves. We have checked the spectra of some known short-period PCEBs (Rebassa-Mansergas et al. 2008; Parsons et al. 2013) based on SDSS and/or LAMOST observations carefully, it is found that most of them exhibit emission features in their optical spectra. This implies that short-period PCEBs might be easily discovered from WDMS binaries with the emission line(s), therefore we attempt to find more PCEBs from about 200 WDMS binaries with emission line(s) at Balmer

series (Silvestri et al. 2007; Rebassa-Mansergas et al. 2010; Liu et al. 2012; Li et al. 2014; Guo et al. 2015; Kepler et al. 2015) through detecting the variability in their luminosities based on the analysis of the photometric data from ZTF survey (Graham et al. 2019; Masci et al. 2019). As a result, it is found that 55 binary systems exhibit variability in their luminosities through the analysis of their light curves, and their orbital periods are found to locate in a range from 2.2643 to 81.1526 hours (listed in Table 1), implying that they are short-period PCEBs. Then we match them with Simbad database, it is found that 6 short-period PCEBs are newly discovered and the orbital periods have been improved for 19 PCEBs. A detailed comparison between the orbital periods obtained by us and their known ones for 49 known PCEBs is shown in Fig. 1. As seen from Fig. 1, the orbital periods derived in this work are consistent with the known periods for 30 short-period PCEBs except that the orbital periods derived by us for 8 PCEBs (displayed by squares) are different from the upper limits of their orbital periods estimated by Morgan et al. (2012) based on several radial velocity (RV) measurements. In addition, the orbital periods obtained for 5 PCEBs (indicated by triangles) by us are only a half of their known ones resulted by an assumption that each full light curve should exhibit two maxima and two minima because of ellipsoidal effect. However we do not find any difference between two maxima or two minima in their light curves when their known periods are used to calculate the phases for their light curves, implying that our results for these PCEBs might be correct, however they must be confirmed by the radial velocity observations in the future. The newly discovered PCEBs, together with 14 PCEBs with an improved orbital period, are as the followings:

### 2.1 Short-period PCEBs with Balmer emission line(s)

#### 2.1.1 SDSS J0029

SDSS J002926.82+252553.90 (hereafter SDSS J0029) was first identified as a DA WD by Skiff (2009), then its atmospheric and physical parameters were derived to be  $T_{\text{eff}} = 19,148(173)$  K,  $\log g = 7.58(3)$  and  $M = 0.459(7)M_{\odot}$  by Kepler et al. (2019) based on the spectrum from SDSS DR14. This suggests that SDSS J0029 is a hot low-mass He-WD which might need a friend to be a short-period PCEB (Marsh, Dhillon & Duck 1995).

Its spectrum from SDSS indicates that this WD should be accompanied by a cool M-type star with the Na I  $\lambda\lambda$  8183.27 and 8194.81 absorption doublet (see Fig. 2). Meanwhile, it is found in Fig. 2 that the H $\alpha$  emission presents in its spectrum. The emission feature may arise due to wind accretion, magnetic activity and/or irradiation because of a hot WD companion, then the reflection effect or star spot (due to magnetic activity) will provide a favorable opportunity for detecting the variability in its luminosity. Thereupon, we collect 724 data points in *g*-band, 975 data points in *r*-band and 133 data points in *i*-band from ZTF DR19 for this object, it is found that the light curves in *g* and *r*-bands exhibit a large scatter which is much larger than their observational uncertainties. This implies that the luminosity of this object might be changed with the time, therefore after some scattered data points are removed, the light curves (720 data points in *g*-band, 953 data points in *r*-band and 131 data points in *i*-band) of this object are analyzed through a code named *Period04* (Lenz & Breger 2005). Its orbital period is derived to be 0.12165200 days in *g*-band, 0.12165254 days in *r*-band or 0.12165232 days in *i*-band and the errors ( $3\sigma$ ) of three periods are derived to be  $5.3 \times 10^{-7}$ ,  $2.7 \times 10^{-7}$  and  $3.3 \times 10^{-7}$  days, respectively. The periodograms indicating the orbital periods for SDSS J0029 are shown in the left panels of Fig. 3. In general, the amplitude of the luminosity variation because

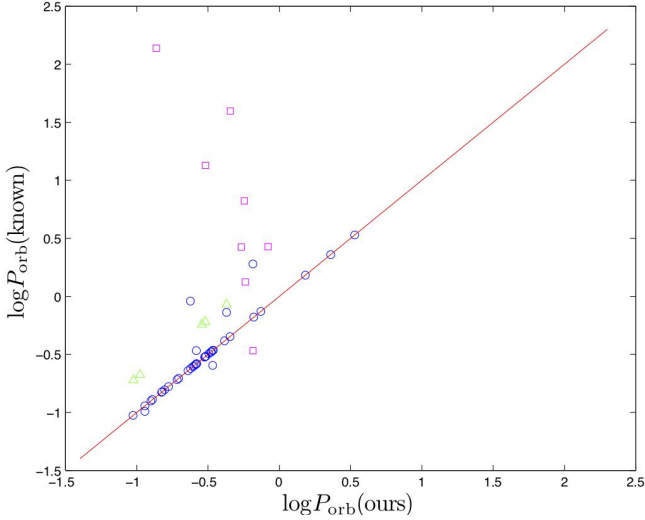


**Figure 1.** A comparison between the known orbital periods and the ones obtained by us for 49 known short-period PCEBs with hydrogen emission line(s) from SDSS or LAMOST. Solid line represents that the orbital periods obtained by us are consistent with the known ones. Squares represent 8 PCEBs with an upper limit in their orbital periods (Morgan et al. 2012), triangles indicate 5 PCEBs with known orbital periods that are twice those given by us and open dots represent other short-period PCEBs.

of reflection effect or spot activity in  $r$ -band is relatively larger than that in  $g$ -band for the PCEBs with a hot WD and an M-type star and thus the orbital period determined by photometric data in  $r$ -band is more accurate than that derived from the observations in  $g$ -band. Therefore, the results on the orbital period derived from  $r$ -band data are listed in Table 1. At last, the phase for each data point is calculated based on an orbital period of 0.12165254 days, the phase-folded light curves are shown in the right top panel of Fig. 3. Meanwhile, as seen from the left panels of Fig. 3, there might be other possible orbital periods for this object that might not be ruled out, since the power is similar for all peaks. Therefore, two possible orbital periods indicated by two peaks near the main peak (the highest one) are derived to be 0.1084267(1) and 0.1385524(2) days respectively based on the  $r$ -band data, and the corresponding light curves are plotted in the medium and bottom panels of the right panels of Fig. 3. As seen from the right panels of Fig. 3, It is difficult to directly find the difference in the light curves based on the different periods. In order to obtain the orbital period for this object, we combine 953 data points into 50 normal points in  $r$ -band observations for three cases mentioned above and calculate their  $\chi^2$ -values (where  $\chi^2 = \frac{1}{N} \sum_i \frac{(r_i - r_{\text{nor},i})^2}{\sigma_i^2}$ , in which  $r_i$  is the magnitude of the  $i$ th data point in  $r$ -band observations,  $r_{\text{nor},i}$  is a magnitude obtained through interpolation in the magnitudes of the normal points based on the phase of the  $i$ th data point and  $\sigma_i$  the observation uncertainty of the  $i$ th data point) which are listed in Table 2. It is found that the  $\chi^2$ -value based on the period indicated by the main peak is a smallest one. This implies that the light curves based on the orbital period indicated by the main peak are most smoothed ones and display fewer scatter data points based on the same photometric data. Therefore, the orbital period of this object should be the one indicated by the main peak in the periodograms of SDSS J0029. This suggests that SDSS J0029 is a short-period PCEBs with an orbital period of about 2.9197 hours.

### 2.1.2 SDSS J0032

SDSS J003221.87+073934.50 (SDSS J0032) was first classified as a PCEB by Schreiber et al. (2010) who gave the atmospheric and physical parameters for this object as the followings:  $T_{\text{eff}} = 21,045$  K,  $M_{\text{WD}} = 0.38M_{\odot}$ ,  $M_s = 0.431M_{\odot}$ ,  $d = 398$  pc, and a peak to peak radial velocity variation of  $298.70 \text{ km s}^{-1}$ . Then these parameters were investigated again by other investigators (e.g. Rebassa-Mansergas et al. 2010; Girven et al. 2011; Kepler et al. 2019).

The WD component of this binary system exhibits a large variability in its radial velocities, implying that SDSS J0032 should be a short-period PCEB. Therefore, we collect the photometric data from ZTF DR19 and find that this object indeed shows an evident change in its luminosity. Using the same method as that used for SDSS J0029, its orbital period is derived to be 0.1539950(14) days and 0.1539945(27) days based on the  $r$  and  $i$ -band data, respectively and the results derived from the  $r$ -band data are also listed in Table 1. Since the periodogram based on  $i$ -band data displays a similar peak distribution to that based on  $r$ -band data, so only one periodogram indicating the orbital period for this object based on the  $r$ -band data is shown in Fig. 4. We also calculate the  $\chi^2$ -values for the main peak and a peak with a frequency of  $5.4910388 \text{ d}^{-1}$  ( $P_{\text{orb}} = 0.1821151$  days) and a similar power to the main one which are also listed in Table 2. It is found in Table 2 that the  $\chi^2$ -value based on a period implied by the main peak is the smaller one. This suggests that the period indicated by the main peak should be its orbital period and its light curves based on an orbital period of 0.15399450 days are shown in Fig. 5(a). It is found in Fig. 5(a) that this object is indeed a short-period PCEB, and the periodic variation in its luminosity might be caused by the reflection effect or spot activity of its MS component.

### 2.1.3 SDSS J0253

SDSS J025301.60-013006.96 (SDSS J0253) was first identified as a DA+M binary based on the spectra from SDSS DR9 by Li et al. (2014). The atmospheric and physical parameters for this object were derived based on the analysis of its spectra from LAMOST and SDSS. It is found that this binary system contains a hot WD and an M-type dwarf (Li et al. 2014; Guo et al. 2015; Kepler et al. 2015; Ren et al. 2018).

It is found in Fig. 2 that this object shows the convincing emissions at  $H\alpha$ ,  $\beta$  and Ca II triplet which might arise from an irradiated component in this object, implying that SDSS J0253 might be a short-period PCEB. Therefore, it is possible that the variability in its luminosity can be detected based on the photometric observations if its orbital inclination is appropriate. In addition, Holl et al. (2023) had found a spurious signal with a frequency of  $1.37165769 \text{ d}^{-1}$  (corresponds to a period of 0.7290448 days) probably related to time-dependent scan angle for this object based on Gaia DR3  $G$ -band time series data. In order to determine whether this spurious period is its orbital period or not, we collect the photometric data from ZTF DR19 to study the variability in the luminosity of SDSS J0253. As a result, the total of 464 data points in  $g$ -band, 476 data points in  $r$ -band and 46 data points in  $i$ -band are obtained. Then the light curves are analyzed after some data points with a large scatter are ignored, its orbital period is derived to be 0.4264210(19) days in  $g$ -band and 0.4264303(15) days in  $r$ -band, respectively and the results are also listed in Table 1, and only one periodogram indicating its orbital period based on  $r$ -band data is shown in Fig. 4 because of the same reason as that for SDSS J0032. Although there is a peak with a similar power to the main one and a frequency of  $1.3423156 \text{ d}^{-1}$  [corresponds to a period of

**Table 1.** The results on analysis of the light curves for 55 PCEBs (the first 25 objects are newly discovered or period corrected PCEBs).

| Stars          | RA<br>(J2000) | Dec<br>(J2000) | $T_{WD}$<br>(K) | $\log g_{WD}$ | $M_{WD}$<br>( $M_{\odot}$ ) | Type   | $P_{orb}$<br>(days) | Errs( $3\sigma$ )<br>( $10^{-5}$ days) | Amplitude<br>(mag) | $P_{orb}^{known}$<br>(days)            | Notes |
|----------------|---------------|----------------|-----------------|---------------|-----------------------------|--------|---------------------|--|--------------------|--|-------|
| SDSS J0029     | 7.36183       | +25.43177      | 19148           | 7.578         | 0.458                       | DA/Me  | 0.12165254          | 0.027                                  | 0.0479             | –                                      | (1)   |
| SDSS J0032     | 8.09105       | +7.65965       | 21045           | 7.43          | 0.38                        | DA/Me  | 0.1539950           | 0.14                                   | 0.0296             | –                                      | (2)   |
| SDSS J0253     | 43.25668      | –1.50177       | 24726           | 7.61          | 0.45                        | DA/Me  | 0.4264303           | 0.15                                   | 0.0374             | 0.72904 <sup>a</sup>                   | (4)   |
| SDSS J0306     | 46.52996      | –0.52066       | 21640           | 7.22          | 0.39                        | DA/Me  | 0.541158            | 5.4                                    | 0.0217             | 2.66 <sup>b</sup>                      | (5)   |
| SDSS J0747     | 116.87735     | +43.06765      | 15964           | 8.37          | 0.85                        | DA/Me  | 0.5781084           | 1.7                                    | 0.0395             | 1.33 <sup>b</sup>                      | (2)   |
| SDSS J0908     | 137.19754     | +61.52831      | 18160           | 8.25          | 0.83                        | DA/Me  | 0.1372305           | 0.07                                   | 0.1974             | 137.43 <sup>b</sup>                    | (6)   |
| SDSS J0927     | 141.80006     | +28.77479      | 22037           | 7.80          | 0.52                        | DA/Me  | 0.3036211           | 0.47                                   | 0.0190             | 13.46 <sup>b</sup>                     | (2)   |
| SDSS J1038     | 159.65513     | +1.84959       | 34332           | 7.56          | 0.47                        | DA/Me  | 0.835045            | 3.5                                    | 0.0125             | 2.68 <sup>b</sup>                      | (7)   |
| SDSS J1424     | 216.73090     | 44.54029       | –               | –             | –                           | WD/K7e | 0.3549873           | 0.29                                   | 0.0141             | –                                      | (2)   |
| SDSS J1541     | 235.33267     | +12.15400      | 25369           | 7.44          | 0.44                        | DA/Me  | 0.1140253           | 0.10                                   | 0.0599             | 0.10232 <sup>c</sup>                   | (8)   |
| LAMOST J1621   | 245.30287     | +41.30261      | 14540           | 7.88          | 0.55                        | DA/Me  | 3.198935            | 9.1                                    | 0.0080             | –                                      | (3)   |
| SDSS J1638     | 249.60319     | +29.45031      | 19000           | 7.5           | 0.39                        | DA/Me  | 0.454168            | 1.6                                    | 0.0230             | 39.49 <sup>b</sup>                     | (9)   |
| SDSS J1705     | 256.32455     | +33.75211      | 34592           | 7.24          | 0.44                        | DA/Me  | 0.3405451           | 0.81                                   | 0.0987             | 0.254066 <sup>c</sup>                  | (2)   |
| SDSS J2130     | 322.58247     | +6.20127       | 34131           | 7.73          | 0.53                        | DA/Me  | 0.2621132           | 0.12                                   | 0.1112             | 0.341167 <sup>c</sup>                  | (1)   |
| SDSS 2208      | 332.20414     | +12.36241      | 86726           | 9.23          | 1.32                        | DA/Me  | 0.654242            | 1.4                                    | 0.0173             | 0.34 <sup>b</sup> , 1.903 <sup>d</sup> | (2)   |
| SDSS J2302     | 345.51029     | –00.15844      | 19416           | 8.02          | 0.63                        | DA/Me  | 0.2376198           | 0.03                                   | 0.1502             | 0.9098531 <sup>f</sup>                 | (1)   |
| SDSS J2320     | 350.01674     | +27.10662      | 31890           | 7.71          | 0.52                        | DA/Me  | 0.794531            | 1.0                                    | 0.0239             | –                                      | (4)   |
| SDSS J2343     | 355.80397     | +15.68515      | 26801           | 7.84          | 0.56                        | DA/Me  | 0.5687399           | 1.06                                   | 0.0192             | 6.64 <sup>b</sup>                      | (2)   |
| SDSS J0950     | 147.68317     | +39.26165      | 41462           | 7.57          | 0.49                        | DA/Me  | 1.167341            | 1.5                                    | 0.0247             | –                                      | (10)  |
| SDSS J1317     | 199.46524     | +67.53313      | 79476           | 6.99          | 0.44                        | DA/Me  | 3.38136             | 20.0                                   | 0.0365             | 3.3820 <sup>a</sup>                    | (2)   |
| SDSS J0803     | 120.76923     | +12.30289      | 15964           | 9.0           | 1.20                        | DA/Me  | 0.2861439           | 0.25                                   | 0.0335             | 0.5723126 <sup>g</sup>                 | (2)   |
| SDSS J0858     | 134.57486     | +39.16987      | –               | –             | –                           | WD/Me  | 0.4268106           | 0.41                                   | 0.0410             | 0.853573 <sup>h</sup>                  | (1)   |
| SDSS J1006     | 151.69061     | +0.53463       | 26104           | 7.21          | 0.39                        | DA/Me  | 0.1055909           | 0.026                                  | 0.1077             | 0.2118 <sup>g</sup>                    | (1)   |
| SDSS J1016     | 154.08253     | –2.04946       | 75536           | 8.40          | 0.91                        | DA/Me  | 0.3025928           | 0.21                                   | 0.0363             | 0.605190 <sup>h</sup>                  | (1)   |
| SDSS J1145     | 176.29077     | +38.22479      | 20000           | 9.0           | 1.20                        | DA/Me  | 0.09501896          | 0.026                                  | 0.0418             | 0.19003799 <sup>g</sup>                | (9)   |
| SDSS J0110     | 17.53785      | +13.43789      | 25360           | 7.40          | 0.41                        | DA/Me  | 0.3326836           | 0.021                                  | 0.0239             | 0.3326867 <sup>g</sup>                 | (11)  |
| SDSS J0314     | 48.71713      | +2.10195       | 41140           | 8.02          | 0.69                        | DA/Me  | 0.3052987           | 0.062                                  | 0.3784             | 0.305297 <sup>g</sup>                  | (3)   |
| SDSS J0836     | 129.07769     | +43.44758      | 24726           | 7.64          | 0.46                        | DA/Me  | 0.1968954           | 0.13                                   | 0.0698             | 0.196898 <sup>g</sup>                  | (2)   |
| LAMOST J090812 | 137.05016     | +6.07252       | 17505           | 7.37          | 0.34                        | DA/Me  | 0.1494378           | 0.083                                  | 0.3273             | 0.149438 <sup>d</sup>                  | (2)   |
| SDSS J0912     | 138.06824     | +23.74517      | 30071           | 8.09          | 0.70                        | DA/Me  | 0.2635584           | 0.14                                   | 0.1225             | 0.2635582 <sup>g</sup>                 | (2)   |
| SDSS J0939     | 144.95038     | +32.96887      | 28389           | 7.75          | 0.52                        | DA/Me  | 0.3309915           | 0.3                                    | 0.0733             | 0.33099 <sup>d</sup>                   | (2)   |
| SDSS J0946     | 146.64359     | +20.50089      | 10307           | 8.04          | 0.63                        | DA/Me  | 0.2528599           | 0.24                                   | 0.0925             | 0.25286122 <sup>g</sup>                | (2)   |
| SDSS J0957     | 149.33022     | +23.71125      | 25891           | 7.55          | 0.43                        | DA/Me  | 0.15087312          | 0.063                                  | 0.1257             | 0.1508707 <sup>g</sup>                 | (2)   |
| SDSS J1000     | 150.06317     | +30.72522      | 14560           | 8.50          | 0.93                        | DA/Me  | 0.4515002           | 0.14                                   | 0.1514             | 0.4514995 <sup>g</sup>                 | (2)   |
| SDSS J1013     | 153.48454     | +27.40292      | 13000           | 9.0           | 1.15                        | DA/Me  | 0.12904056          | 0.02                                   | 0.1514             | 0.12904 <sup>d</sup>                   | (6)   |
| SDSS J1106     | 166.61528     | –1.08741       | 30071           | 7.46          | 0.42                        | DA/Me  | 0.4134605           | 0.53                                   | 0.0140             | 0.413462 <sup>g</sup>                  | (2)   |
| SDSS J1108     | 167.02231     | +65.36985      | 21045           | 7.53          | 0.41                        | DA/Me  | 0.3208369           | 0.35                                   | 0.1063             | 0.3208343 <sup>g</sup>                 | (2)   |
| SDSS J1157     | 179.43685     | +48.93838      | 11567           | 8.00          | –                           | DA/Me  | 2.29114             | 22.0                                   | 0.0438             | 2.2911685 <sup>g</sup>                 | (1)   |
| SDSS J1226     | 186.62876     | +30.64795      | 30071           | 7.41          | 0.400                       | DA/Me  | 0.2586904           | 0.23                                   | 0.1107             | 0.258687 <sup>g</sup>                  | (2)   |
| SDSS J1239     | 189.76222     | +65.82626      | 21470           | 7.76          | 0.50                        | DA/Me  | 0.661913            | 1.2                                    | 0.0528             | 0.6619085 <sup>g</sup>                 | (11)  |
| LAMOST J1249   | 192.49901     | +3.95736       | 53842           | 7.28          | 0.42                        | DA/Me  | 0.743405            | 1.5                                    | 0.0214             | 0.743407 <sup>i</sup>                  | (10)  |
| SDSS J1348     | 207.17369     | +18.56961      | 16000           | 8.0           | 0.62                        | DA/Me  | 0.2484319           | 0.18                                   | 0.1063             | 0.24843148 <sup>g</sup>                | (6)   |
| SDSS J1408     | 212.19603     | +29.84608      | 30000           | 7.75          | 0.52                        | DA/Me  | 0.19179001          | 0.09                                   | 0.0944             | 0.1917903 <sup>g</sup>                 | (6)   |
| SDSS J1411     | 212.89464     | +10.4778       | 30419           | 7.74          | 0.52                        | DA/Me  | 0.1675101           | 0.06                                   | 0.1763             | 0.1675099 <sup>g</sup>                 | (2)   |
| SDSS J1415     | 213.90176     | +1.28836       | 73816           | 8.43          | 0.96                        | DA/Me  | 0.3443278           | 0.44                                   | 0.0672             | 0.34433084 <sup>g</sup>                | (2)   |
| SDSS J1435     | 218.94948     | +37.56086      | 12392           | 7.61          | 0.41                        | DA/Me  | 0.12563074          | 0.043                                  | 0.0844             | 0.1256311 <sup>g</sup>                 | (2)   |
| LAMOST J1439   | 219.94843     | –1.10189       | 76410           | 7.97          | 0.73                        | DA/Me  | 1.522581            | 8.2                                    | 0.0212             | 1.522608 <sup>g</sup>                  | (2)   |
| SDSS J1456     | 224.14262     | +16.19379      | 20000           | 7.50          | 0.44                        | DA/Me  | 0.2291217           | 0.14                                   | 0.0180             | 0.2291202 <sup>g</sup>                 | (6)   |
| SDSS J1519     | 229.77486     | +50.11747      | 31270           | 7.66          | 0.49                        | DA/Me  | 0.3023353           | 0.24                                   | 0.0444             | 0.30236455 <sup>g</sup>                | (11)  |
| SDSS J1539     | 234.90879     | +27.10162      | 36572           | 7.31          | 0.40                        | DA/Me  | 0.2385547           | 0.05                                   | 0.0438             | 0.238553 <sup>g</sup>                  | (2)   |
| SDSS J1559     | 239.76931     | +3.93978       | 48770           | 7.98          | 0.68                        | DA/Me  | 0.09434753          | 0.012                                  | 0.0363             | 0.0943473 <sup>g</sup>                 | (2)   |
| SDSS J1620     | 245.12053     | +63.07967      | 23551           | 7.12          | 0.31                        | DA/Me  | 0.2994283           | 0.32                                   | 0.482              | 0.299429 <sup>i</sup>                  | (7)   |
| LAMOST J1724   | 261.02585     | +56.33405      | 37999           | 7.15          | 0.37                        | DA/Me  | 0.3330190           | 0.13                                   | 0.1039             | 0.333028 <sup>h</sup>                  | (13)  |
| SDSS J1730     | 262.51038     | +33.56718      | 49042           | 7.345         | 0.42                        | DA/Me  | 0.1569469           | 0.086                                  | 0.1571             | 0.1569473 <sup>g</sup>                 | (12)  |
| SDSS J2123     | 320.83431     | +5.71489       | 21045           | 7.82          | 0.54                        | DA/Me  | 0.26204957          | 0.071                                  | 0.1215             | 0.2620477 <sup>g</sup>                 | (1)   |

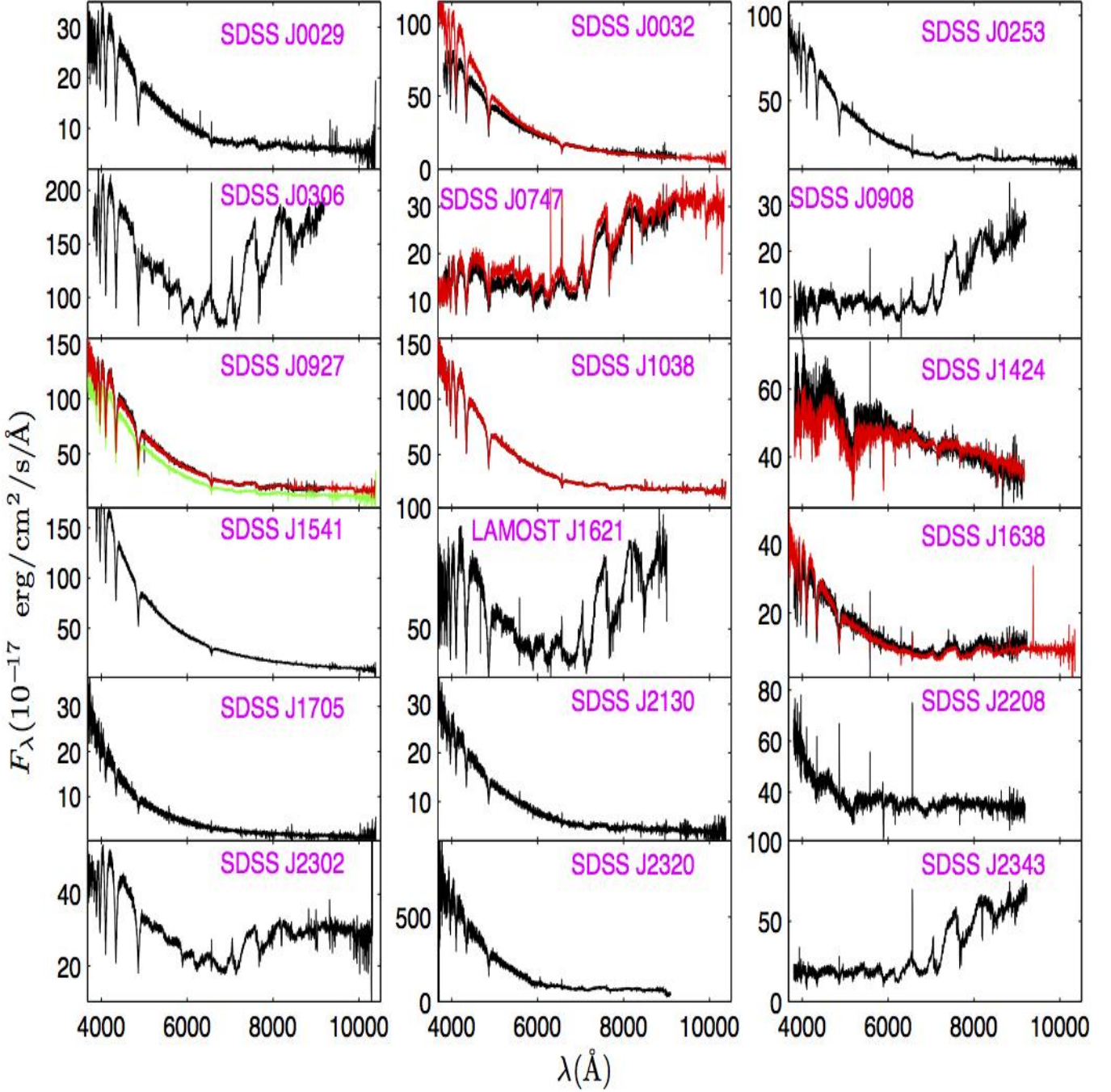


**Figure 2.** The optical spectra for short-period PCEBs with hydrogen emission line(s) from SDSS or LAMOST. The different colours indicate the different available spectra.

0.7449813(89) days] based on Fig. 4, which is still different from the signal frequency obtained by Holl et al. (2023), so the period of the signal discovered by Holl et al. (2023) might be a spurious signal related to time-dependent scan angle rather than the orbital period of this object. Meanwhile, it is found in Table 2 that the  $\chi^2$ -value based the period indicated by the main peak is also smaller than that derived from this peak, implying that the period indicated by the main peak is the orbital period of this object. The phase-folded light curves in  $g$ ,  $r$  and  $i$ -bands are drawn in Fig. 5(b), and the variability in its luminosity is caused by the reflection effect or star spot.

#### 2.1.4 SDSS J0306

SDSS J030607.19-003114.44 (SDSS J0306, also named KUV03036-0043) was first observed spectroscopically by KISO Schmidt ultraviolet excess survey and then was classified as a DA+dM binary (Weger, McMahan & Boley 1987). Subsequently the different atmospheric and physical parameters for the DA star in this object had been obtained by the various investigators, it was found that this WD might be a He-WD (Schreiber et al. 2010; Debes et al. 2011) or a C/O-WD (Tremblay et al. 2011; Limoges & Bergeron 2010; Morgan et al.

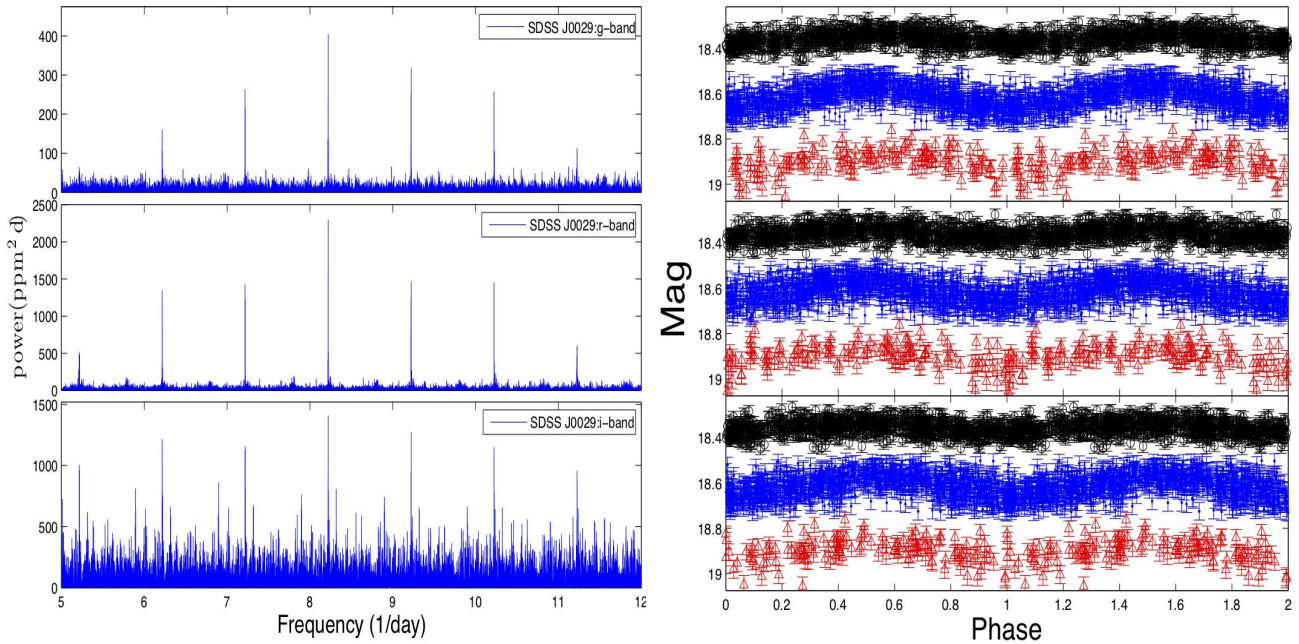


**Figure 3.** The periodograms indicating orbital periods and the phase folded light curves for SDSS J0029 based on the ZTF *g*, *r* and *i*-band photometric observations, respectively.

2012; Rebassa-Mansergas et al. 2010; Gianninas, Bergeron & Ruiz 2011). Although KUV 03036-0043 was identified as a WD+M4/M5 binary by Raymond et al. (2003) and Kleinman et al. (2013), however it was argued as a close binary by Silvestri et al. (2007) and Morgan et al. (2012) who estimated an upper limit of 2.66 days for the orbital period of this object based on several RV measurements.

The radial velocities were determined for the DA WD component by some previous investigators (Schreiber et al. 2010; Rebassa-Mansergas et al. 2010; Morgan et al. 2012; Dietz et al. 2020). It was found that its radial velocity exhibits a large peak to peak variation (about  $273.30 \text{ km s}^{-1}$ , Schreiber et al. 2010). Meanwhile, Balmer emission lines are evidently presented in its optical spectra (see Fig. 2), they might be caused by magnetic activity or irradiation of M-type dwarf due to its hot WD companion. These observational characteristics suggest that KUV 03036-0043 might be a short-period PCEB which provides a favorable opportunity for researchers to observe the variability in its luminosity. So we collect the photometric data from ZTF DR19 to investigate the variability in the luminosity of SDSS J0306. As a result, the total 422 data points in *g*-band and 428 data points in *r*-band are obtained. After some data points with a large scatter are neglected, the light curves are analyzed. As the objects mentioned above, only one periodogram indicating its orbital period based on *r*-band data is also shown in Fig. 4. Meanwhile, the  $\chi^2$ -values are obtained for its *r*-band light curves based on two orbital periods indicated by the main peak and another peak with a similar power to the main one and a frequency of  $2.8505955 \text{ d}^{-1}$  ( $P_{\text{orb}} = 0.3508039 \text{ days}$ ) and they are also listed in Table 2. It is found in Table 2 that the  $\chi^2$ -value based on the orbital period indicated by the main peak is also a smaller one, suggesting that the period implied by the main peak should be its orbital period, then its orbital period is derived to be  $0.541179(65) \text{ days}$  in *g*-band and  $0.541158(54) \text{ days}$  in *r*-band, respectively. Its phase-fold light curves are displayed in Fig. 5(c). As seen from Fig. 5(c), this object is a short-period PCEB with an orbital period of about 12.9878 hours, and its luminosity change might be caused by star spot due

to magnetic activity or reflection effect. In addition, the orbital period obtained for this object by us is indeed smaller than its upper limit listed in Morgan et al. (2012), suggesting that the orbital period obtained for this object might be correct.

### 2.1.5 SDSS J0747

SDSS J074730.57+430403.65 (SDSS J0747) was first identified as WD+dM binary according to its spectrum from SDSS by Raymond et al. (2003). The atmospheric and physical parameters for this object were obtained through a analysis of the spectrum from SDSS (Schreiber et al. 2010; Rebassa-Mansergas et al. 2010). It was found that this object is a DA+M4/M5 binary (West et al. 2008; Kleinman et al. 2013). The radial velocities for SDSS J0747 were analyzed by Rebassa-Mansergas et al. (2010) and Schreiber et al. (2010) who gave a peak to peak radial velocity variation of  $328.90 \text{ km s}^{-1}$ . This suggests that SDSS J0747 might be a short-period PCEB. Meanwhile, Balmer emission lines evidently present in its optical spectra from SDSS, this also indicates that SDSS J0747 might be a short-period PCEB and they might arise due to magnetic activity or irradiation of the cool component by a hot WD (more than 15,000 K, Rebassa-Mansergas et al. 2010; Schreiber et al. 2010).

The radial velocities were derived to be  $-487.6(248.4)$  and  $177.0(417.7) \text{ km s}^{-1}$  for M-type dwarf and WD components respectively by Morgan et al. (2012) who also estimated an upper limit of 1.33 days for the orbital period of this object, suggesting that the variability in its luminosity might be detected. In order to find the variability in its luminosity, we collect the photometric data for it from ZTF DR19, the total 570 data points in *g*-band and 2394 data points in *r*-band are obtained, the light curves are also analyzed after some data points with a large scatter are removed, and the periodogram manifesting the orbital period for SDSS J0747 is also displayed in Fig. 4. The  $\chi^2$ -values derived for the *r*-band light curves based on the orbital periods indicated by the main peak and another peak with a frequency of  $0.2728867 \text{ d}^{-1}$  ( $P_{\text{orb}} = 3.66453$

**Table 2.** The  $\chi^2$ -values derived for different periods indicated by different peaks in periodograms for the newly discovered or period-improved PCEBs. The period indicated by the main peak is highlighted as bold for each PCEB.

| Stars      | frequencies<br>(d <sup>-1</sup> ) | Periods<br>(days) | Amplitude<br>(mag) | $\chi^2$ | Stars        | frequencies<br>(d <sup>-1</sup> ) | Periods<br>(days) | Amplitude<br>(mag) | $\chi^2$ |
|------------|-----------------------------------|-------------------|--------------------|----------|--------------|-----------------------------------|-------------------|--------------------|----------|
| SDSS J0029 | 8.2201419                         | <b>0.12165254</b> | 0.0479             | 1.7488   | SDSS J1145   | 10.52421538                       | <b>0.09501896</b> | 0.0418             | 7.5294   |
|            | 9.2228990                         | 0.1084257         | 0.0382             | 1.8842   |              | 12.52693508                       | 0.07982799        | 0.0336             | 9.4481   |
|            | 7.2173656                         | 0.1385524         | 0.0377             | 2.95117  |              |                                   |                   |                    |          |
| SDSS J0032 | 6.4937663                         | <b>0.1539945</b>  | 0.0296             | 0.9183   | SDSS J1317   | 0.295739                          | <b>3.38136</b>    | 0.0365             | 2.7320   |
|            | 5.4910338                         | 0.1821151         | 0.0293             | 1.9262   |              | 0.7042455                         | 1.419959          | 0.0309             | 3.3896   |
| SDSS J0253 | 2.3450291                         | <b>0.4264303</b>  | 0.0374             | 0.9480   | SDSS J1424   | 2.8170022                         | <b>0.3549873</b>  | 0.0141             | 2.8010   |
|            | 1.3423156                         | 0.744981          | 0.0343             | 1.0685   |              | 3.8169625                         | 0.2619884         | 0.0138             | 4.3389   |
| SDSS J0306 | 1.8478892                         | <b>0.541158</b>   | 0.0217             | 4.8067   | SDSS J1541   | 8.7699835                         | <b>0.1140253</b>  | 0.0599             | 2.2010   |
|            | 2.8505955                         | 0.3508039         | 0.0194             | 4.8270   |              | 9.7699776                         | 0.1023554         | 0.0384             | 6.6393   |
| SDSS J0747 | 1.7297794                         | <b>0.5781084</b>  | 0.0395             | 38.9850  | LAMOST J1621 | 0.312604                          | <b>3.198935</b>   | 0.0080             | 2.9878   |
|            | 0.2728867                         | 3.66453           | 0.0321             | 48.0663  |              | 0.6901616                         | 1.448936          | 0.0072             | 3.1978   |
| SDSS J0803 | 3.4947451                         | <b>0.2861439</b>  | 0.0335             | 3.0446   | SDSS J1638   | 2.2018283                         | <b>0.454168</b>   | 0.0230             | 1.4888   |
|            | 4.4975074                         | 0.2223454         | 0.0322             | 4.6632   |              | 3.2045401                         | 0.3120573         | 0.0193             | 2.3150   |
| SDSS J0858 | 2.3429596                         | <b>0.4268106</b>  | 0.0410             | 3.5121   | SDSS J1705   | 2.9364686                         | <b>0.3405451</b>  | 0.0987             | 1.7059   |
|            | 4.3457009                         | 0.2301125         | 0.03333            | 6.7661   |              | 3.9391781                         | 0.2538601         | 0.0847             | 1.7308   |
| SDSS J0908 | 7.2870098                         | <b>0.1372305</b>  | 0.1974             | 11.5378  | SDSS J2130   | 3.8151455                         | <b>0.2621132</b>  | 0.1112             | 3.8770   |
|            | 6.2843572                         | 0.1591253         | 0.1025             | 46.4421  |              | 2.8123848                         | 0.3555701         | 0.0952             | 7.2091   |
| SDSS J0927 | 3.2935787                         | <b>0.3036211</b>  | 0.0190             | 1.7210   | SDSS J2208   | 1.5284864                         | <b>0.654242</b>   | 0.0173             | 3.7707   |
|            | 5.2962706                         | 0.1888121         | 0.0177             | 2.2048   |              | 0.525674                          | 1.90232           | 0.0170             | 4.2671   |
| SDSS J0950 | 0.8566477                         | <b>1.167341</b>   | 0.0247             | 1.8047   | SDSS J2302   | 4.2084351                         | <b>0.2376198</b>  | 0.1502             | 84.0070  |
|            | 2.8594254                         | 0.3497206         | 0.0212             | 1.9146   |              | 3.2057117                         | 0.3119432         | 0.1417             | 245.3586 |
| SDSS J1006 | 9.47051308                        | <b>0.1055909</b>  | 0.1077             | 4.1035   | SDSS J2320   | 1.258604                          | <b>0.794531</b>   | 0.0239             | 2.2884   |
|            | 7.4677665                         | 0.1339088         | 0.1055             | 9.9490   |              | 0.255855                          | 3.90845           | 0.0170             | 2.3862   |
| SDSS J1016 | 3.3047713                         | <b>0.3025928</b>  | 0.0363             | 1.9146   | SDSS J2343   | 3.3526                            | <b>0.5687399</b>  | 0.0192             | 1.3381   |
|            | 4.3075007                         | 0.2321532         | 0.0341             | 3.2178   |              | 0.7555755                         | 1.323494          | 0.0158             | 1.9402   |
| SDSS J1038 | 1.1975403                         | <b>0.835045</b>   | 0.0125             | 1.2491   |              |                                   |                   |                    |          |
|            | 3.2002366                         | 0.3124769         | 0.0116             | 1.7343   |              |                                   |                   |                    |          |

**Table 3.** The photometric data for SDSS J1541.

| Bands           | Wave length<br>( $\mu\text{m}$ ) | Magnitude<br>(mag) | Flux<br>( $\mu\text{Jy}$ ) |
|-----------------|----------------------------------|--------------------|----------------------------|
| $u'$            | 0.3572                           | 16.830(7)          | 699.8(4.5)                 |
| $g'$            | 0.4640                           | 16.809(4)          | 684.7(2.5)                 |
| $r'$            | 0.6185                           | 17.174(5)          | 488.8(22.0)                |
| $i'$            | 0.7439                           | 17.398(7)          | 393.0(2.5)                 |
| $z'$            | 0.8897                           | 17.533(17)         | 343.4(5.3)                 |
| $g$             | 0.4810                           | 16.886(5)          | 639.1(2.9)                 |
| $r$             | 0.6155                           | 17.250(8)          | 457.1(3.4)                 |
| $i$             | 0.7503                           | 17.579(6)          | 337.6(1.9)                 |
| $z$             | 0.8668                           | 17.742(20)         | 290.5(5.3)                 |
| $y$             | 0.9613                           | 17.176(28)         | 297.6(7.5)                 |
| $G$             | 0.5858                           | 17.032(4)          | 501.0(1.8)                 |
| $G_{\text{bp}}$ | 0.5044                           | 16.967(8)          | 588.0(4.3)                 |
| $G_{\text{rp}}$ | 0.7692                           | 17.164(15)         | 344.8(4.7)                 |
| $W_1$           | 3.3526                           | 16.428(67)         | 276.1(16.5)                |
| $W_2$           | 4.6028                           | 16.299(205)        | 192.9(33.1)                |

days) are also listed in Table 2. As seen from Table 2, the  $\chi^2$ -value based on the main peak is a smaller one. This suggests that the period

indicated by the main peak should be the orbital period of this object. Its orbital period is thus derived to be 0.5781084(17) days in  $r$ -band and the result is listed in Table 1. The phase-folded light curves of SDSS J0747 are plotted in Fig. 6(a). It is found in Fig. 6(a) that this object should be an eclipsing PCEB with a short orbital period of about 13.875 hours. In addition, the orbital period determined for this object is indeed smaller than its upper limit listed in Morgan et al. (2012), also implying that the orbital period derived for this object might be correct.

### 2.1.6 SDSS J0908

SDSS J090847.38+613141.43 (hereafter SDSS J0908) was first identified as a WDMS by Morgan et al. (2012), then the atmospheric and physical parameters for the DA star in this binary system were given as the followings:  $T_{\text{WD}} = 11,000\text{K}$ ,  $\log g = 8.25$ ,  $M_{\text{WD}} = 0.827M_{\odot}$ ,  $V_{\text{WD}} = 37.6 \text{ km s}^{-1}$  and  $V_{\text{dM}} = -124.6 \text{ km s}^{-1}$ . Another estimation for the radial velocity of DA WD in this object was  $-40.436 \pm 28.598 \text{ km s}^{-1}$  (Tsantaki et al. 2022). These works indicate that this object might be a short-period PCEB.

An upper limit on the orbital period for this object was estimated to be 137.43 days by Morgan et al. (2012). However, as seen Fig. 2, the

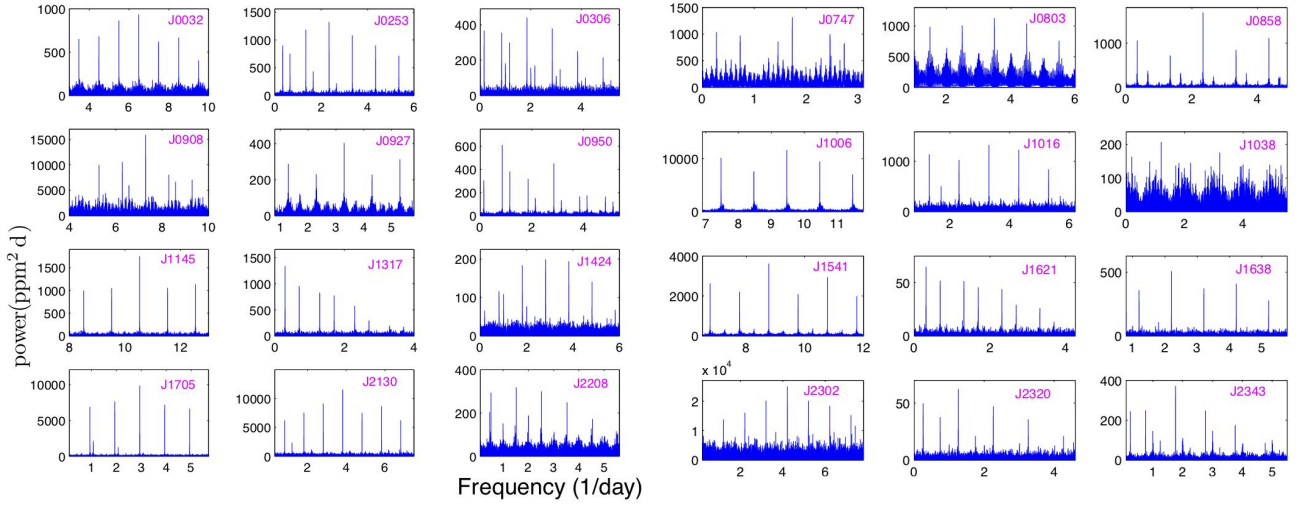


**Figure 4.** The periodograms indicating orbital periods derived from *r*-band ZTF photometric observations for newly discovered or period-corrected PCEBs (only SDSS J2320 based on *g*-band observations).

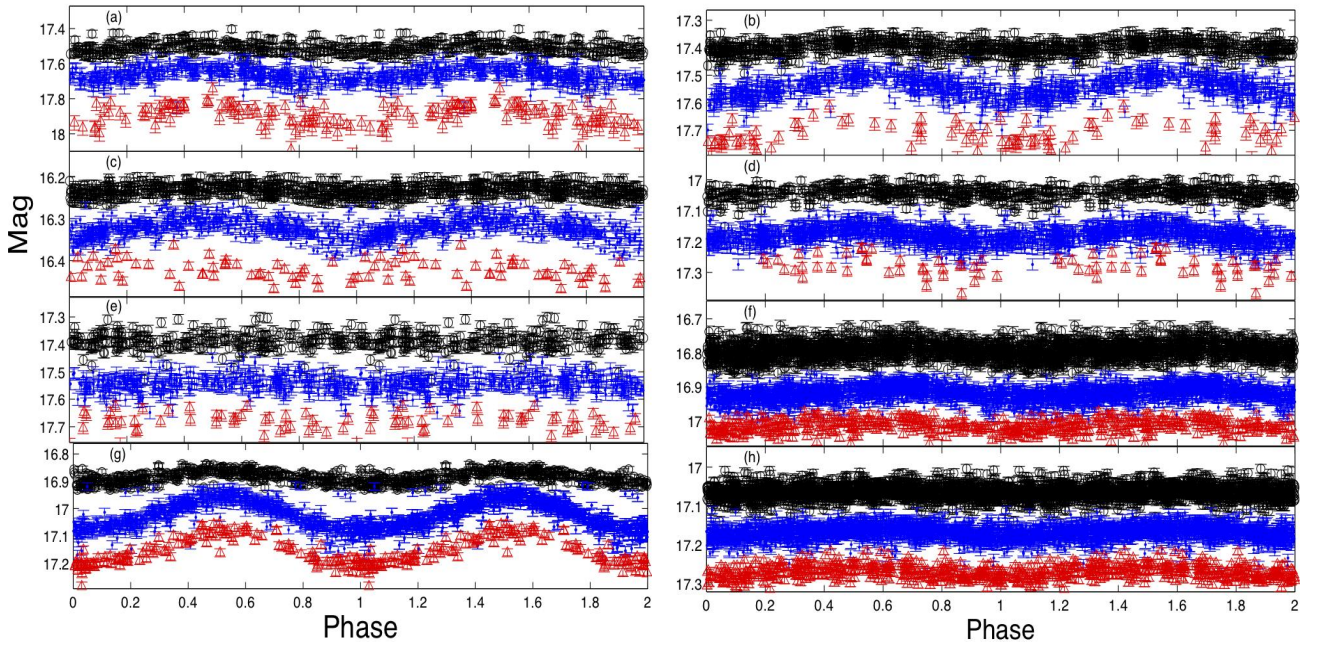


**Figure 5.** The light curves in *g*, *r* and *i*-bands for 8 PCEBs only with hydrogen emission line(s). In each panel, black open dots represent the *g*-band observations, the blue solid dots indicate the *r*-band observations, and the red open triangles represent the *i*-band ones.

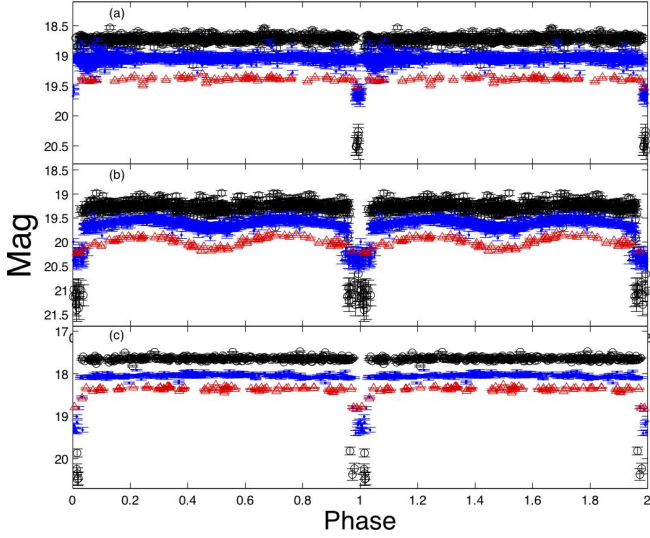
Balmer emission lines also arise in the optical spectrum from SDSS, this suggests that this object might be a short-period PCEB. In order to obtain the accurate period for it, we collect the photometric data from ZTF DR19 for SDSS J0908, then the total 649 data points in *g*-band and 780 data points in *r*-band are obtained. The light curves of SDSS J0908 are analyzed through the same method as that mentioned above, and only one periodogram indicating the orbital period for SDSS J0908 based on *r*-band is also shown in Fig. 4. As seen from Fig. 4, it is difficult to rule out some possible orbital periods indicated by other peaks with a similar power to the main peak. In order to find the orbital period for this object, we calculate the  $\chi^2$ -values for the *r*-band light curves based on the periods indicated by the main peak and another peak with a frequency of  $6.2843572 \text{ d}^{-1}$  ( $P=0.1591253$  days), which are listed in Table 2. It is found in

Table 2 that the  $\chi^2$ -value based on the main peak is also a smaller one, implying that the period indicated by the main peak should be the orbital period of this object, then its orbital period is derived to be  $0.1372302(10)$  days in *g*-band,  $0.1372305(7)$  days in *r*-band, respectively and the results are listed in Table 1. Its phase-folded light curves for SDSS J0908 are shown in Fig. 6(b). It is found in Fig. 6(b) that SDSS J0908 should be also a close eclipsing PCEB. Meanwhile, the orbital period derived for this object is much smaller than its upper limit estimated by Morgan et al. (2012).

### 2.1.7 SDSS J0927

SDSS J092712.02+284629.28 (SDSS J0927) was first suspected to be a DA WD by Pesch & Sandulek (1983), then it was identified as





**Figure 6.** Same as Fig. 5, but for three eclipsing PCEBs (SDSS J0747, SDSS J0908 and SDSS J2302) .

a DA WD by [Wagner et al. \(1988\)](#). Thereafter, it was reclassified as a DA/M binary (e.g. [Kleinman et al. 2013](#); [Guo et al. 2015](#)). The atmospheric and physical parameters for both components of this object were derived based on the analysis of the spectra from LAMOST or SDSS ([Rebassa-Mansergas et al. 2010](#); [Gianninas, Bergeron & Ruiz 2011](#); [Morgan et al. 2012](#); [Guo et al. 2015](#)). The atmospheric and physical parameters were derived to be  $T_{\text{eff}} = 22,037$  K,  $\log g = 7.80$ , and  $M_{\text{WD}} = 0.52M_{\odot}$  by [Rebassa-Mansergas et al. \(2010\)](#) who gave a distance of 237 pc away from the Earth, which is closest to a distance of about  $235.4 \pm 5.5$  pc indicated by its parallax from *Gaia* DR3 ([Gaia Collaboration 2021](#)). The radial velocities of two components in SDSS J0927 were derived to be  $-73.5$  and  $133.1$   $\text{km s}^{-1}$  for the M-type star and DA star, respectively ([Morgan et al. 2012](#)) who estimated an upper limit of 13.46 days for the orbital period of this object, this suggests that this object might be a PCEB.

$H\alpha$  emission line is evidently presented in its optical spectra from SDSS and LAMOST (see Fig. 2), this also implies that this object might be a short-period PCEB. We also collect the photometric data for SDSS J0927 from ZTF DR19. As a result, the total of 356 data points in  $g$ -band and 758 data points in  $r$ -band are obtained. Then the light curves are also analyzed after some data points with a large scatter are neglected. Its orbital period is determined to be 0.3036308(63) days in  $g$ -band and 0.3036211(47) days in  $r$ -band, respectively. The results are listed in Table 1 and only one periodogram based on  $r$ -band data is shown in Fig. 4. As the same as the objects mentioned above, we have to calculate the  $\chi^2$ -values for its  $r$ -band light curves based on the different orbital periods indicated by the main peak and another peak with a similar power to the main peak (see Table 2). The results suggest that the period indicated by the main peak should be the orbital period of this object, then the phase-folded light curves for SDSS J0927 are displayed in Fig. 5(d). As seen from Fig. 5(d), SDSS J0927 should be a PCEB with an orbital period of about 7.287 hours. In addition, the orbital period obtained for this object is indeed smaller than its upper limit given by [Morgan et al. \(2012\)](#) and thus might be correct.

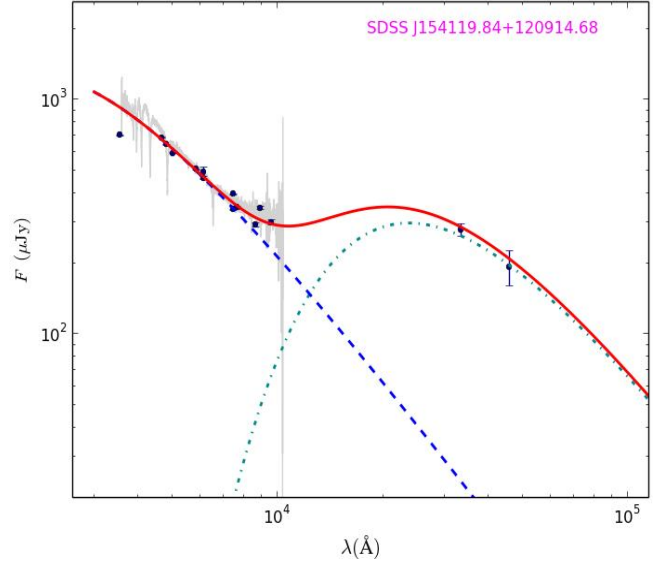


**Figure 7.** The fitting result of SED of SDSS J1541 based on the atmospheric parameters obtained in this work. Solid dots represent the observed fluxes derived from the photometric magnitudes, the dashed line (blue) indicates the contribution of the white dwarf, and the dot-dashed line (darkcyan) means the contribution of a cool dwarf. The solid line (red) represents the contribution of both white dwarf and M-type dwarf, the gray line denotes its observed spectrum from SDSS.

#### 2.1.8 SDSS J1038

SDSS J103837.22+015058.48 (hereafter SDSS J1038) was classified as a close WD+MS binary by [Silvestri et al. \(2006\)](#) based on the spectra from SDSS DR4. Its atmospheric and physical parameters had been obtained by other investigators based on the spectra from SDSS (e.g. [Rebassa-Mansergas et al. 2010](#); [Debes et al. 2011](#); [Tremblay et al. 2011](#); [Morgan et al. 2012](#); [Kleinman et al. 2013](#); [Bedard et al. 2020](#)). Thereafter, these parameters were derived from the optical spectrum from LAMOST by [Ren et al. \(2018\)](#) who gave the similar results as those based on the spectra from SDSS. The radial velocities for both components of this object were derived to be  $-180.4$  and  $157.4$   $\text{km s}^{-1}$  for the M-type star and WD respectively by [Morgan et al. \(2012\)](#) who also estimated an upper limit of 2.68 days for the orbital period of this object based on several RV measurements, this implies that this object might be a short-period PCEB. In order to find its accurate period, we collect the photometric data for this object from ZTF DR19 to investigate the variability in its luminosity. The total of 233 data points in  $g$ -band and 345 data points in  $r$ -band are obtained, then the light curves of SDSS J1038 are analyzed if some data points with a large scatter are not taken into account and the periodogram implying the orbital period for this object is displayed in Fig. 4. As seen from Fig. 4, there are some peaks with a similar power to the main peak in its periodogram, we must calculate the  $\chi^2$ -values for its  $r$ -band light curves based on the periods indicated by the main peak and another peak with a frequency of  $3.2002366$   $\text{d}^{-1}$  (corresponding to  $P_{\text{orb}}=0.3124769$  days), which are listed in Table 2. It is found in Table 2 that the  $\chi^2$ -value based on the main peak is the smaller one, suggesting that the period indicated by the main peak should be the orbital period. At last, its orbital period is derived to be 0.835045(35) days according to the photometric data in  $r$ -band and its phase-folded light curves are shown in Fig. 5(e). As seen from Fig. 5(e), SDSS J1038 is a short-period PCEB although the amplitude of the variation in its luminosity is small because of

a small orbital inclination. Meanwhile, the orbital period obtained for this object by us is really smaller than its upper limit given by [Morgan et al. \(2012\)](#) and thus should be correct.

### 2.1.9 SDSS J1424

SDSS J142417.74+443225.00 (SDSS J1424) was identified as a WD+MS binary by [Heller et al. \(2009\)](#) and [Rebassa-Mansergas et al. \(2010\)](#) because of its ultraviolet excess. The effective temperature of the main sequence component in this object was derived to be 5116(72) K ([Miller 2015](#)) or 5206 K ([Tonry et al. 2018](#)), which corresponds to an effective temperature of a  $\sim$ K1-type dwarf ([Bell & Gustafsson 1989](#)). The radial velocities of this object were determined as 55.00 (Na I) or 36.50 (H $\alpha$ ) km s<sup>-1</sup> based on SDSS spectrum ([Rebassa-Mansergas et al. 2010](#)). Another radial velocity for this object was derived to be 319.27 km s<sup>-1</sup> based on Gaia BP/RP spectrum ([Verberne et al. 2024](#)), suggesting that SDSS J1424 shows a large variability in its radial velocity and thus might be a short period PCEB.

Meanwhile, H $\alpha$  emission line is also evidently presented in its optical spectra (see Fig. 2), this also implies that this object might be a short-period PCEB. In order to find its orbital period, we collect the photometric data for this object from ZTF DR19, and analyze its light curves in *g*, *r* and *i*-bands. An orbital period is derived to be 0.3549873(29) days for SDSS J1424 from its *r*-band photometric data and the periodogram implying its orbital period is shown in Fig. 4. It is also difficult to rule out some possible periods indicated by the peaks with a similar power to the main one for this object based on Fig. 4. By using the same method as that used for the objects mentioned above, it is found that the period indicated by the main peak should be the orbital period of this object (see Table 2). At last, its phase-folded light curves are shown in Fig. 5(f). It is found in Fig. 5(f) that SDSS J1424 is indeed a short period PCEB with an orbital period of about 8.5187 hours.

### 2.1.10 SDSS J1541

SDSS J154119.84+120914.68 (SDSS J1541) was first identified as a DA WD by [Girven et al. \(2011\)](#) who had given the effective temperature [ $T_{\text{eff}} = 19,000$  K] and surface gravity [ $\log g = 8.50$ ] based on a spectrum obtained by SDSS on 2011 June 25. These spectral parameters of SDSS J1541 were improved by [Kepler et al. \(2015\)](#) and [Kepler et al. \(2019\)](#), who gave the effective temperature [ $T_{\text{eff}} = 25,464(129)$  K], surface gravity [ $\log g = 7.480(16)$ ], and mass [ $M_{\text{WD}} = 0.454(6) M_{\odot}$ ] for this object based on the same spectrum as that used in [Girven et al. \(2011\)](#). It is found in Fig. 2 that the emission lines are evidently presented at H $\alpha$  and Ca II triplet, suggesting that this object should be accompanied by a cool star. The spectral features of this object are almost dominated by its WD companion. Apart from emission characteristics of the companion star, its other spectral features are difficultly found out from the spectrum of this object. Therefore, it is necessary to obtain the properties of its cool companion by analyzing the spectral energy distribution (SED) of this object. However, there is an evident difference in its spectral parameters provided by previous investigators, thus we have to verify its spectral parameters through spectral analysis since the result of SED analysis strongly depends on the spectral and physical parameters of the WD component. By using of a grid of WD model atmospheres ([Koester 2010](#)), we analyzed its SDSS spectrum again under an assumption that the WD has redshift owing to proper motion and strong gravity of this object, we obtained the effective temperature [ $T_{\text{eff}} = 25,369(142)$  K], surface gravity [ $\log g = 7.44(2)$ ] and

a radial velocity [ $51.0(\pm 4.0)$  km s<sup>-1</sup>] for this object. we derived the mass [ $M_{\text{WD}} = 0.44(1) M_{\odot}$ ], cooling age [ $\tau_c = 45.8 \pm 3.9$  Myr], and radius [ $R_{\text{WD}} = 0.0208(4) R_{\odot}$ ] for this WD on the basis of a recently updated version of the cooling models ([Bergeron et al. 1995](#)).

At last, based on a well known equation  $d = \sqrt{\frac{\pi R_{\text{WD}} [R_{\odot}]^3}{a}}$  (where  $a = F_{\text{obs},\lambda} / F_{\text{ast},\lambda}$  is a ratio of the observed spectral flux on the earth to the astrophysical flux at the stellar surface, [Heller et al. 2009](#)), the spectroscopic distance of this WD is estimated to be of 369( $\pm 9$ ) pc away from the Earth, which is consistent with a distance of 370.3 $\pm$ 8.3 pc derived through its parallax (2.7003 $\pm$ 0.0636, [Gaia Collaboration 2021](#)). These results are in good agreement with those derived by [Kepler et al. \(2015, 2019\)](#).

Based on the ZTF photometric data, this object was discovered a variable star with an orbital period of 0.10232 days in *g*-band and 0.11403 days in *r*-band ([Chen et al. 2020](#)). This also suggests that this object should not be a single white dwarf, but a binary containing a hot DA star. Meanwhile, we fit its H $\alpha$  emission line by using a Gaussian profile in detail, the radial velocity of its cool component is derived to be  $-183.0 \pm 1.3$  km s<sup>-1</sup>, which is much higher than that of WD (+51(4) km s<sup>-1</sup> in this work, and 19(4) km s<sup>-1</sup> in [Kepler et al. 2019](#)). Therefore, the mass of its companion should be much lower than that of the DA star.

In order to obtain the properties of the cool component of SDSS J1541, it is necessary to investigate the SED of SDSS J1541 based on the photometric magnitudes from optical to infrared bands. The optical photometric magnitudes are obtained from SDSS DR7 (*u'g'r'i'z'*, [Abazajian et al. 2009](#)), Gaia DR3 (*GG<sub>bp</sub>G<sub>rp</sub>*, [Gaia Collaboration 2021](#)) and Pan-StrRRs DR1 (*grizy*, [Chambers et al. 2016](#)). The near-infrared (near-IR) photometry data are taken from WISE (*W<sub>1</sub>* and *W<sub>2</sub>*, [Wright et al. 2010](#)). The magnitude and flux density in each passband for SDSS J1541 are listed in Table 3, and they are plotted in Fig. 7 with solid dots. As seen from Fig. 7, SDSS J1541 indeed shows IR excesses from *z*-band to *W<sub>2</sub>*, and thus this hot WD should be accompanied a cool companion.

IR excesses of WDs are usually explained by the existence of a debris disk or a cool companion (a cool dwarf or even a planet). The parameters of the cool component of WDs are usually derived based on the SED analysis through a least  $\chi^2$  methods ([Girven et al. 2011](#), and references therein). Using this method, the SED of SDSS J1541 is analyzed, then the temperature and radius for its cool component are derived to be 2,018(207) K and 0.438 $R_{\odot}$ , corresponding to a late M-type star with a mass of about 0.080 $M_{\odot}$  according to an effective-mass relationship with an age of 5 Gyr ([Baraffe et al. 2003](#); [Rebassa-Mansergas et al. 2007](#)). Therefore SDSS J1541 is a short-period PCEB composed of a hot WD and a late M-type dwarf. Although the orbital period for this object has been derived by [Chen et al. \(2020\)](#), however there is a difference (about 17 min) between a period determined by *g*-band data and another one based on *r*-band data. We collect the photometric data from ZTF DR19, and obtain 375 data points in *g*-band, 605 data points in *r*-band and 133 data points in *i*-band, respectively. Then the light curves are analyzed through a method used in SDSS J0029, and only one periodogram implying its orbital period based on *r*-band data is shown in Fig. 4. Its orbital period is derived to be 0.1140249(11) days in *g*-band, 0.1140253(10) days in *r*-band and 0.1140261(11) in *i*-band, respectively, and the results are also listed in Table 1. The light curves based on an orbital period determined by *r*-band data for SDSS J1541 are displayed in Fig. 5(g). It is found in Fig. 5(g) that SDSS J1541 is a PCEB with an orbital period of about 2.7366 hrs and the variation in its luminosity might be caused by reflection effect or a dark spot due to stellar activity. Our results on the orbital period of this object are in well

agreement with that derived by [Chen et al. \(2020\)](#) based on  $r$ -band data, and a different orbital period derived for this object by them based on  $g$ -band data might be caused by an selection of wrong peak due to scattered data points or fewer data points in  $g$ -band at that time. In fact, it is found in Fig. 4 that a signal with a similar power to main peak and a frequency of  $9.769997632 \text{ d}^{-1}$ , corresponds to an orbital period of 0.102355417 days, which is in agreement with that given by [Chen et al. \(2020\)](#) based on  $g$ -band data. This suggests that the scattered data points or the number of all data points might lead to a wrong peak selection. Meanwhile, it is found in Table 2 that  $\chi^2$ -value according to the period indicated by the main peak is smaller than that based this peak, suggesting that the orbital period should be the period indicated by the main peak as the objects mentioned above.

### 2.1.11 LAMOST J1621

LAMOST J162112.62+411809.81 (also named KUV 16195+4125) was first observed spectroscopically by the KISO Schmidt ultraviolet excess survey and discovered as a DA+dM binary ([Weger & Swanson 1990](#)). After that, it was found that this binary system can be resolved with Hubble Space telescope ([Farihi et al. 2006](#)). The atmospheric and physical parameters for the DA star were derived to be  $T_{\text{eff}} = 14,090(457) \text{ K}$ ,  $\log g = 7.93(6)$  and  $M_{\text{WD}} = 0.57_{\odot}$  ([Limoges & Bergeron 2010](#)). The similar results had been obtained again by other investigators based on the spectra from KISO or LAMOST ([Gianninas, Bergeron & Ruiz 2011](#); [Guo et al. 2015](#); [Ren et al. 2018](#)).

Meanwhile, it is found in Fig. 2 that the emission feature at  $H\alpha$  also can be seen from its LAMOST spectrum clearly, implying that this object might be a close PCEB and thus the variability in its luminosity might be detected through photometric observations. We collect the photometric data from ZTF DR19 for it, the total of 1330 data points in  $g$ -band, 1321 data points in  $r$ -band and 379 data points in  $i$ -band are obtained. The light curves are analyzed and only one periodogram indicating its orbital period based on  $r$ -band data is displayed in Fig. 4 and the results are listed in Table 1. In addition, it is found in Table 2 that the  $\chi^2$ -value derived for its  $r$ -band light curve based on the period indicated by the main peak is smaller than that based on a peak with a similar power to the main one and a frequency of  $0.6901616 \text{ d}^{-1}$  (corresponding to a period  $P = 1.448936$  days), so that the period indicated by the main peak should be its orbital period, then the orbital period is derived to be 3.198935(91) days in  $r$ -band and 3.200093(145) days in  $i$ -band, respectively. then the light curves based on the orbital period determined by photometric observations in  $r$ -band are displayed in Fig. 5(h). It is found in Fig. 5(h) that LAMOST J1621 indeed exhibits the periodic variation in its luminosity with a short period and is thus a PCEB with a short orbital period. The variability in the luminosity of LAMOST J1621 might be a result of reflection effect or a star spot owing to magnetic activity.

### 2.1.12 SDSS J1638

SDSS J163824.78+292701.23 (hereafter SDSS J1638) was first classified as a DA+dM binary by [Skiff \(2009\)](#), then the atmospheric and physical parameters for the components of this object were derived by [Rebassa-Mansergas et al. \(2010\)](#) and [Liu et al. \(2012\)](#). It was found that SDSS J1638 is composed of a hot DA WD and a  $0.32M_{\odot}$  M-type dwarf. Thereafter, these parameters were derived by [Ren et al. \(2018\)](#) again based on its spectrum from LAMOST.

The radial velocities for the DA star and M dwarf were determined to be  $-51.6$  and  $123.9 \text{ km s}^{-1}$  respectively by [Morgan et al. \(2012\)](#) who gave an upper limit of 39.49 days for the orbital period of this object based on the RV observations without multi-epoch measurements, suggesting that SDSS J1638 might be a short-period PCEB and the variability in its luminosity might be detected based on the photometric observations. In order to obtain its actual orbital period for this object, we collect the photometric observations for it from ZTF DR19, the total of 1028 data points in  $g$ -band, 1148 data points in  $r$ -band and 160 data points in  $i$ -band, respectively. However, its orbital period can be only derived from the photometric observations in  $r$ -band and it is 0.454168(16) days (listed in Table 1) and the periodogram indicating its orbital period is also shown in Fig. 4. As seen from Fig. 4, there are some possible periods that can not be ruled out, however. It is found in Table 2 that the  $\chi^2$ -value based on the main peak is also smaller than that based on another peak with a similar power to the main one and a frequency of  $3.2045401 \text{ d}^{-1}$  ( $P = 0.3120573$  days), suggesting that the period indicated by the main peak is the orbital period of this object. Then three light curves are plotted in Fig. 8(a). As seen from Fig. 8(a), SDSS J1638 shows periodic variation in its luminosity evidently and it should be a short period PCEB. The variability in the luminosity of SDSS J1638 might be caused by the reflection effect or a star spot due to stellar activity of the M-type dwarf. Meanwhile, the orbital obtained for this object in this work is really shorter than its upper limit listed in [Morgan et al. \(2012\)](#), suggesting that it might be correct.

### 2.1.13 SDSS1705

SDSS170517.87+334507.61 (hereafter SDSS J1705) was classified as a DA white dwarf by [Elsenstein et al. \(2006\)](#) based on the spectra from SDSS DR4. Then it was found to be a binary system containing a WD and a cool companion by [Silvestri et al. \(2007\)](#) and the DA star in this binary system was found to be very hot one by [Kleinman et al. \(2013\)](#) and [Anguiano et al. \(2017\)](#). A radial velocity of the DA star was derived to be  $-47.78 \text{ km s}^{-1}$ , and the distance was estimated to be 1685.9 pc away from the the Earth which is consistent with a distance of  $2027.6 \pm 864.1$  pc indicated by its parallax from Gaia DR3. Another radial velocity of this object was estimated to be  $292.08 \text{ km s}^{-1}$  from the redshift based on its LAMOST spectrum ([Zhang et al. 2022](#)), suggesting that this object might show a large variability in its radial velocity and thus a short period PCEB.

Based on the photometric data from ZTF DR2, the orbital periods for this object were derived to be 0.254066 days in  $g$ -band and 0.34053 days in  $r$ -band by [Chen et al. \(2020\)](#), suggesting that it is necessary to find the true orbital period for this object because the different periods were given by [Chen et al. \(2020\)](#) based the photometric data from different passbands. The light curves based on the photometric data from ZTF DR19 is analyzed again and only one periodogram implying its orbital period based on  $r$ -band data is shown in Fig. 4. Its orbital periods are determined as 0.3405506(97) days in  $g$ -band, 0.3405451(81) days in  $r$ -band and 0.3405535(137) days in  $i$ -band, respectively. Our results are in well agreement with a period determined by [Chen et al. \(2020\)](#) based on ZTF  $r$ -band data, and a different orbital period derived by [Chen et al. \(2020\)](#) from  $g$ -band data might be a result of a selection of wrong peak owing to the less data points in  $g$ -band at that time or the influence of some scattered data points. In fact, it is found in Fig. 4 that a peak with a similar power to the main one and a frequency of  $3.9391472 \text{ d}^{-1}$  (corresponds to an orbital period of 0.2538621 days) is in agreement with the peak which was used to derive its orbital period based on ZTF  $g$ -band data by [Chen et al. \(2020\)](#). However, the  $\chi^2$ -value based

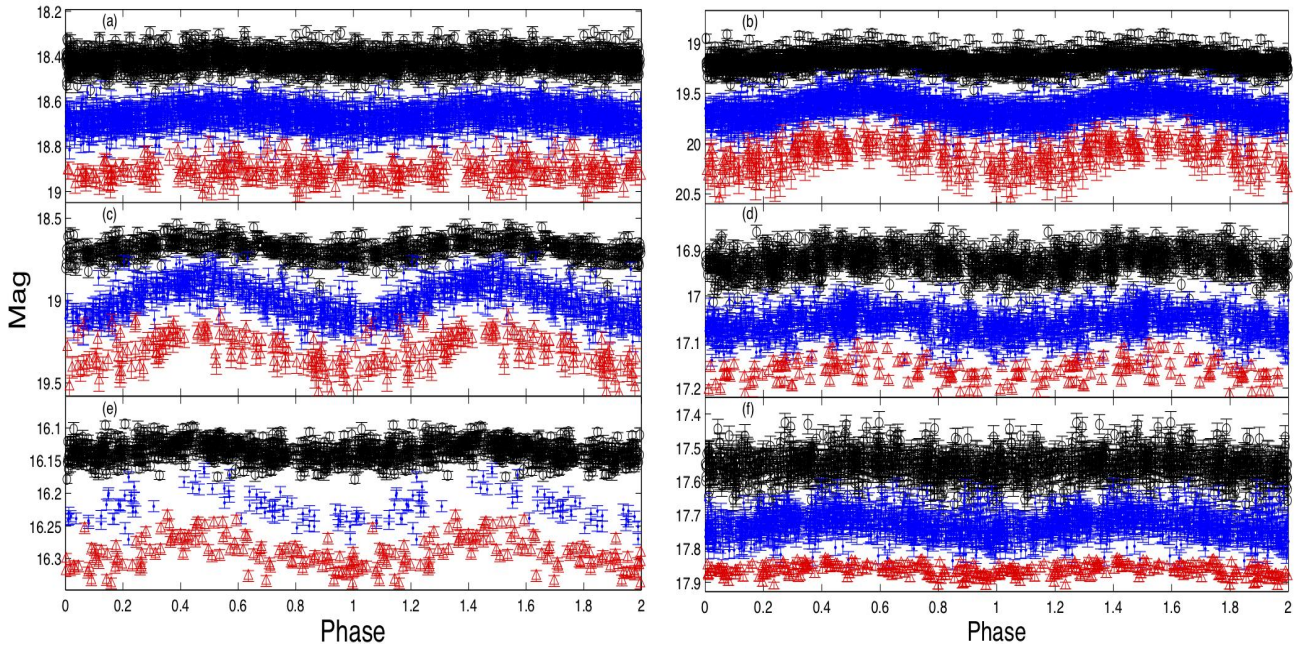


**Figure 8.** Same as Fig. 5. But for other 6 PCEBs (i.e. SDSS J1638, SDSS J1705, SDSS J2130, SDSS J2208, SDSS J2320, and SDSS J2343).

on this peak is larger than that based on main one (see Table 2), which implies that the period indicated by the main peak is the orbital period of this object, then its three phase-folded light curves are displayed in Fig. 8(b).

#### 2.1.14 SDSS J2130

SDSS J213019.79+061204.58 (SDSS J2130) was first identified as a WD+MS binary by [Gentile Fusillo, Gänsicke & Greiss \(2015\)](#) and [Kepler et al. \(2015\)](#) who gave the atmospheric and physical parameters for the WD in this object as the followings:  $T_{\text{eff}} = 34, 131\text{K}$ ,  $\log g = 7.730$  and  $M_{\text{WD}} = 0.534M_{\odot}$ . This object was classified as a RR Lyr-type variable with a pulsation period of 0.34116743 days by [Sesar et al. \(2017\)](#) and [Gavras et al. \(2023\)](#).

Meanwhile, the hydrogen Balmer emission lines are also presented in its SDSS spectrum (see Fig. 2), and thus suggests that SDSS J2130 might be a short period PCEB. In order to obtain the orbital period for this object, we collect the photometric data for it from ZTF DR19, then the light curves in  $g$ ,  $r$  and  $i$ -bands are analyzed, however only one periodogram implying its orbital period is shown in Fig. 4 since the periodograms obtained from photometric observations in  $g$  and  $i$ -bands for this object show the similar peak distribution to that derived from  $r$ -band data. Meanwhile, as the objects mentioned above, the period indicated by the main peak in Fig. 4 should be the orbital period of this object since the  $\chi^2$ -value based on the main peak is smaller than that based on another peak with a similar power and a frequency of  $2.8123848\text{ d}^{-1}$ , corresponding a period of 0.355574 days (see Table 2), therefore its orbital period is derived to be 0.2621130(14), 0.2621132(12) and 0.2621115(14) days according to  $g$ ,  $r$  and  $i$ -band photometric data, respectively. Its phase-folded light curves are shown in Fig. 8(c). As seen from Fig. 8(c), three light curves show the same trend of change, implying that this object should be a short period PCEB with an orbital period of about 6.2907 hours. Although we attempt to find a peak with a similar power to the main one and a period matching its known period obtained by [Sesar et al. \(2017\)](#) and [Gavras et al. \(2023\)](#), however we do not find any

peak that can satisfy the requirements from Fig. 4, suggesting that a different orbital period obtained for this object by [Sesar et al. \(2017\)](#) and [Gavras et al. \(2023\)](#) is not a result of the selection of a wrong peak.

#### 2.1.15 SDSS J2208

SDSS J220849.00+122144.73 (SDSS J2208) was first classified as a WD+MS binary by [Silvestri et al. \(2007\)](#) based on its spectrum from SDSS DR5. The atmospheric and physical parameters for the DA star in this object were obtained by previous investigators (e.g. [Rebassa-Mansergas et al. 2010](#); [Morgan et al. 2012](#)). It was found that the DA WD in SDSS J2208 is a massive one and the radial velocities for both components were derived to be  $31.10\text{ km s}^{-1}$  for the DA star and  $11.70\text{ km s}^{-1}$  for the M star by [Rebassa-Mansergas et al. \(2010\)](#). Meanwhile, Balmer emission lines are presented in its spectrum from SDSS. These observational characteristics indicate that SDSS J2208 might be a short-period binary formed from common envelope evolution.

An orbital period was estimated to be 0.34 days by [Morgan et al. \(2012\)](#) based on RV measurements without multi-epoch, another different orbital period of 1.903 days was determined by [Ritter & Kolb \(2003\)](#) and [Gavras et al. \(2023\)](#) for this object according to the photometric data from SDSS or ASAS. In order to find the accurate period for SDSS J2208, we collect the photometric observations for it from ZTF DR19, the total of 655 data points in  $g$ -band, 925 data points in  $r$ -band and 96 data points in  $i$ -band are obtained, then the light curves are analyzed and only one periodogram indicating its orbital period based on  $r$ -band data is also shown in Fig. 4. In addition, it is found in Table 2 that the  $\chi^2$ -value based on the main peak is smaller than that based on another peak with a similar power to the main one, implying that the period indicated by the main peak is the orbital period of this object, then its orbital period is derived to be 0.654228(21) days in  $g$ -band and 0.654242(14) days in  $r$ -band, respectively. Three light curves based on an orbital period derived from the  $r$ -band data are displayed in Fig. 8(d). It is found in Fig. 8(d)

that this object should be a short-period PCEB. However, the orbital periods obtained for this object by us or Ritter & Kolb (2003) are longer than its upper limit listed in Morgan et al. (2012), this might be caused by its upper limit resulted by the unsuitable RV measurements ( $V_{\text{dM}} = -323.3$  and  $V_{\text{WD}} = 323.3 \text{ km s}^{-1}$ , Morgan et al. 2012). In addition, an orbital period derived for this object by Ritter & Kolb (2003) and Gavras et al. (2023) might be a result of the selection of a wrong peak. In fact, it is found in Fig. 4 that an period indicated by a peak with a similar power to main one and a frequency of  $0.52567394 \text{ d}^{-1}$  ( $P=1.90232$  days) is in agreement with that used to derive period for this object by Ritter & Kolb (2003) and Gavras et al. (2023).

#### 2.1.16 SDSS J2302

SDSS J230202.50-000930.04 (SDSS J2302) was first identified as DA/M binary based on a spectrum from SDSS DR9 by Li et al. (2014) who gave the atmospheric and physical parameters for both components of SDSS J2302. Then these parameters were studied again by Kepler et al. (2015) and it was found to be a DA+M3 binary. Meanwhile, SDSS J2302 was found to be a variable star with an orbital period of 0.9098531 days by Ivezić et al. (2007). This implies that SDSS J2302 might be a PCEB.

We collect the photometric data for this binary system from ZTF DR19 to obtain the accurate period, the total of 330 data points in  $g$ -band, 360 data points in  $r$ -band and 71 data points in  $i$ -band are obtained, respectively, then the light curves of this object are analyzed, then the periodogram indicating its orbital period based on  $r$ -band data is also shown in Fig. 4. As the objects mentioned above, the  $\chi^2$ -values listed in Table 2 also suggest that the period indicated by the main peak in Fig. 4 is the orbital period of this object, then its orbital period is derived to be 0.2376133(5) days in  $g$ -band and 0.2376198(3) days in  $r$ -band, respectively. At last, the three light curves based on an orbital period obtained from  $r$ -band data are shown in Fig. 6(c). It is found in Fig. 6(c) that SDSS J2302 should be an eclipsing PCEB with an orbital period of about 5.703 hrs, implying that its orbital periods derived by us are very different from that derived by Ivezić et al. (2007). We attempt to find out a peak indicating a period that can match its known period, however, we do not find any peak that meet the requirements from Fig. 4, suggesting that the difference between its known period and our results is not a result of a wrong peak selection, and might be caused by the limited number of the repeated observations ( $\sim 10$ ) adopted by Ivezić et al. (2007) and thus an eclipsing binary with a much shorter duration than its orbital period could easily escape detection (Ivezić et al. 2007).

#### 2.1.17 SDSS J2320

SDSS232004.02+270623.73 (SDSS J2320) was first identified as a DA white dwarf by Oswalt, Peterson & Foltz (1984), and then was reclassified as a DA+M binary by Guo et al. (2015). The atmospheric and physical parameters for the DA star in SDSS J2320 were derived to be  $T_{\text{eff}} = 31,480(491) \text{ K}$ ,  $\log g = 7.68(6)$ ,  $M = 0.50M_{\odot}$  and a distance away from the earth about 246 pc by Limoges & Bergeron (2010) based on the spectrum from KISO Schmidt survey. A similar result about these parameters was obtained again according to the spectrum from LAMOST DR5 by Ren et al. (2018) who gave an M4-type dwarf in this object.

The emission lines at Balmer series are presented in its optical spectra from LAMOST (Guo et al. 2015), implying that this object might be a short-period PCEB. Therefore, the variability in its luminosity might be detected, we collect the photometric data from

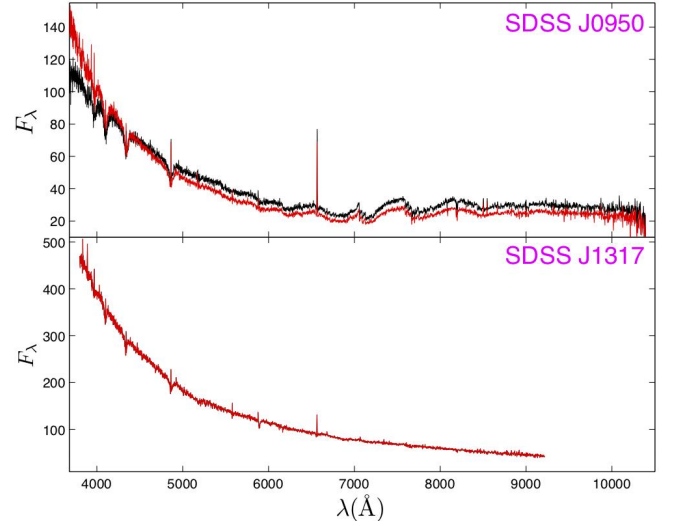


**Figure 9.** Same as Fig.2, but for two short-period PCEBs (SDSS J09500 and SDSS J1317) with He I emission lines. The different colours indicate the different available spectra and  $F_{\lambda}$  in the same units as that in Fig. 2.

ZTF DR19 to discover whether the luminosity of SDSS J2320 is variable or not. As a result, the total of 641 data points in  $g$ -band, 78 data points in  $r$ -band and 111 data points in  $i$ -band are found out for it. Then the light curves are analyzed and only one periodogram indicating its orbital period based on  $g$ -band data is also shown in Fig. 4. As the objects mentioned above, the  $\chi^2$ -values listed in Table 2 also imply that the period indicated by the main peak should be the orbital period of this object, then its orbital period is derived to be 0.794569(12) days in  $g$ -band and 0.794531(10) days in  $i$ -band, respectively. At last, three light cures based on an orbital period derived from  $g$ -band data (a more data point set) are plotted in Fig. 8(e). As seen from Fig. 8(e), three light curves exhibit the same trend in its luminosity change, implying that the orbital period obtained in this work is accurate at present.

#### 2.1.18 SDSS J2343

SDSS234312.96+154106.43 (SDSS J2343) was first identified as a WD+MS binary by Silvestri et al. (2007), and its atmospheric and physical parameters for this object had been studied by the previous investigators (e.g. Rebassa-Mansergas et al. 2010; Morgan et al. 2012). It was found that the DA star in SDSS J2343 is a massive WD with a distance of 225 pc away from the earth (Rebassa-Mansergas et al. 2010). The radial velocities were derived to be  $93.5 \text{ km s}^{-1}$  and  $-224.3 \text{ km s}^{-1}$  for the DA star and M-type star, respectively by Morgan et al. (2012) who also estimated an upper limit of 6.64 days for orbital period of this object based on several RV measurements, suggesting that SDSS J2343 might be a PCEB.

Since its optical spectrum from SDSS exhibits evident emission features at Balmer series (see Fig. 2). This also indicates that SDSS J2343 might be a short-period PCEB, and thus the variation in its luminosity might be detected. We collect the photometric data for SDSS J2343 from ZTF DR19, the total of 663 data points in  $g$ -band, 896 data points in  $r$ -band and 171 data points in  $i$ -band are obtained, respectively. Its light cures are analyzed and only one periodogram indicating its orbital period based on  $r$ -band data is also shown in Fig. 4. Although there are some peaks with a similar power to the main peak in Fig. 4, the period indicated by the main peak should

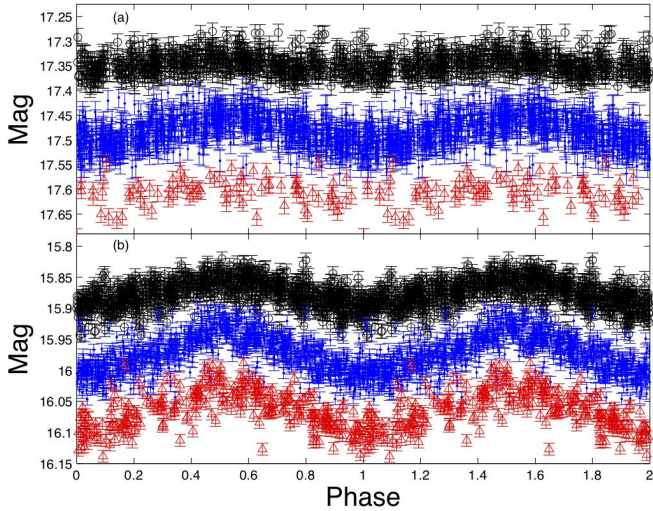


**Figure 10.** Same as Fig. 5, but for two short-period PCEBs (SDSS J0950 and SDSS J1317) with He I emission feature.

be the orbital period of this object based on the  $\chi^2$ -values listed in Table 2 as the same reason as that for the objects mentioned above, then its orbital period is derived to be 0.5687198(130) days in  $g$ -band and 0.5687399(106) days in  $r$ -band respectively and the light curves based on an orbital period determined by the  $r$ -band observations are shown in Fig. 8(f). As seen from Fig. 8(f), SDSS J2343 is indeed a short-period PCEB and the periodic change in its luminosity might be caused by the reflection effect or dark spot due to magnetic activity. In addition, the orbital period obtained for this object is indeed shorter than its upper limit derived by Morgan et al. (2012), and thus might be correct.

## 2.2 Short-period PCEBs with Hydrogen and He I emission features

### 2.2.1 SDSS J0950

SDSS J095043.94+391541.62 (SDSS J0950) was first identified as a WD+MS binary system by Kleinman et al. (2004), then its atmospheric and physical parameters were determined through spectral analysis by many investigators (e.g. Rebassa-Mansergas et al. 2010; Tremblay et al. 2011; Debes et al. 2011; Li et al. 2014; Bedard et al. 2020). These results imply that this binary system should contain a very hot young WD component. Meanwhile, it is found in Fig. 9 that its SDSS optical spectra display not only the strong emission lines at hydrogen Balmer series, but also the emission lines at He I  $\lambda\lambda 5876$  and  $\lambda\lambda 6681$ , together with Ca II H,K. These emission lines exhibit a narrow single peak, implying that SDSS J0950 shows the same emission features as LAMOST J143947.62-010606.8 with an orbital period of about 1.522608 days (Gavras et al. 2023).

We collect the photometric data for this object from ZTF DR19, and analyze its light curves in  $g$  and  $r$ -bands after some scattered data points are removed. The result is listed in Table 1 and only one periodogram implying its orbital period based on  $r$ -band is shown in Fig. 4. For the same reasons as those alleged for the objects mentioned above, the period implied by the main peak is the orbital period of this object (see Table 2), then the orbital period of this object is derived to be 1.167186(21) and 1.167341(15) days based on  $g$  and  $r$ -band data, respectively. The phase of each datapoint in  $g$ ,  $r$  and  $i$ -bands is

calculated according to an orbital period derived from  $r$ -band data, then its phase-folded light curves are shown in Fig. 10(a). As seen from Fig. 10(a), SDSS J0950 is composed of a hot WD and an M-type dwarf with an orbital period of 1.167341 days, and is therefore a detached binary system, rather than a cataclysmic variable.

### 2.2.2 SDSS J1317

SDSS J131751.72+673159.36 (SDSS J1317) was identified as a cataclysmic variable by Green, Schmidt & Liebert (1986). The atmospheric and physical parameters were determined based on its SDSS spectrum by Rebassa-Mansergas et al. (2010); Tremblay et al. (2011) and Bedard et al. (2020). It was found that this WD/MS binary system should be composed of a hot DA WD and an M-type dwarf. The radial velocities were determined to be 460.4(22.5) and -449.2(35.8) km s<sup>-1</sup> at different epochs by Pourbaix et al. (2005), this implies that this object might be a close binaries.

Meanwhile, it is found in Fig. 9 that its SDSS optical spectrum displays not only the strong emission lines at hydrogen Balmer series, but also the emission lines at He I  $\lambda\lambda 5876$  and  $6681$  and each emission line shows a single peak, the emission features in its spectrum are similar to those in the spectra of BE UMa (with  $P_{\text{orb}} = 2.2909892$  days, Sánchez-Sáez et al. 2023) and HK Leo (with  $P_{\text{orb}} = 1.7598817$  days, Gavras et al. 2023). In addition, Holl et al. (2023) discovered a spurious signal with a frequency of 0.29568185 d<sup>-1</sup> (corresponding to a period of 3.382013 days) related to time-dependent scan angle for this object according to Gaia DR3  $G$ -band time series data. In order to find whether this spurious period is the orbital period of this object, we collect the photometric data from ZTF DR19, then analyze the light curves in  $g$ ,  $r$  and  $i$ -bands, the result is listed in Table 1 and the periodogram implying its orbital period from  $r$ -band observations is also shown in Fig. 4. For the same reason as those for SDSS J0029, the period indicated by the main peak in Fig. 4 should be the orbital period of this object (see Table 2), then its orbital period is derived to be 3.38084(20), 3.38136(32) and 3.38115(61) days based on  $g$ ,  $r$  and  $i$ -band data, respectively. The phase for each data point in three passbands is calculated according to a period obtained from  $g$ -band data, then the phase-folded light curves are displayed in Fig. 10(b). This suggests that the period discovered for this object by Holl et al. (2023) should be the orbital period rather than the spurious period for SDSS J1317.

## 3 DISCUSSION AND CONCLUSIONS

The common envelope evolution is one of the most uncertain processes in binary evolution (Politano & Weiler 2007; Nebot Gómez-Morán et al. 2009). The post common envelope binaries (PCEBs) are the direct products of common envelope evolution and thus play an important role in understanding common envelope evolution of binaries (Paczynski 1976; Taam & Sandquist 2000; Nebot Gómez-Morán et al. 2009; Rebassa-Mansergas et al. 2007). In this work, we attempt to discover some PCEBs from WDMS binaries with emission line(s) identified from LAMOST and/or SDSS based on the photometric data from ZTF DR19. As a result, 55 PCEBs with an orbital period within a range from 2.2643 to 81.1526 hours are found out based on the photometric data, however most of them had been discovered by previous investigators. In these short-period PCEBs, 6 of them are newly discovered and the orbital periods of 19 PCEBs have been improved (see the first 25 objects in Table 1) based on a match with Simbad database. A detailed comparison between our results and those obtained by previous investigators is shown in Fig. 1. As seen

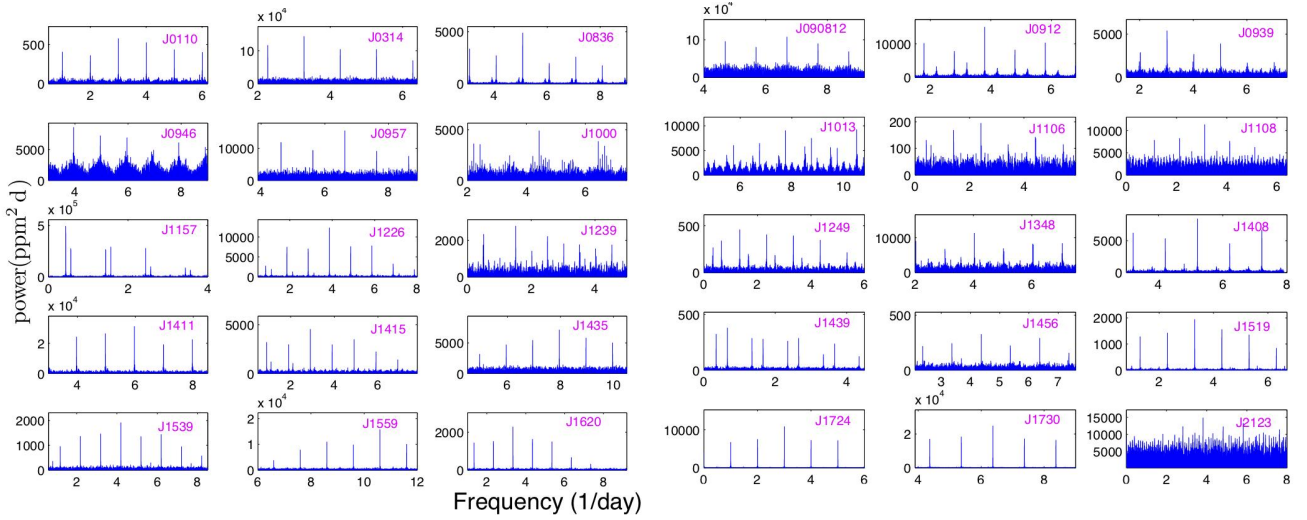


**Figure 11.** The periodograms indicating orbital periods derived from  $r$ -band ZTF photometric observations for 30 PCEBs with an accurate orbital period.

from Fig. 1, our results are consistent with their known ones for most of the known short period PCEBs except for 8 PCEBs (indicated by squares) with the upper limits of their orbital periods (Morgan et al. 2012), implying that the method (named *Period04*, Lenz & Breger 2005) used in this work is effective although almost all periodograms indicating the orbital periods for these short period PCEBs show several peaks with a similar power, because the similar phenomena also occur in the periodograms for 30 short period PCEBs with an accurate period (see Fig. 11). A possible explanation for this phenomenon is that the orbital periods of these binary stars are obtained from the discontinuous observation data from ZTF, which might produce some spurious signals.

It is found in Fig. 4 and Fig. 11 that there are some peaks with a similar power to the main one and thus some possible periods for these PCEBs can not be directly ruled out. In order to find the orbital periods for the newly discovered or period improved PCEBs, we use a  $\chi^2$ -method to check the deviation degree of the phase-folded light curves based on two orbital periods indicated by the main peak and another peak with a similar power to the main one from the ‘averaged’ light curves constructed by 50 normal points. It is found in Table 2 that the deviation degree of light curve based on the orbital period indicated by the main peak is lower than that of light curve based on another peak for each of them, suggesting that the periods indicated by the main peaks in their periodograms are their orbital periods, also suggesting that the method used in this work is effective. In addition, some peaks with a similar power to the main one in their periodograms might be a result of a small amplitude of light variation in these short period PCEBs composed of a WD and a low-mass dwarf, and the limited repeated observations or scattered data points would lead to select a wrong peak for some binaries (such as SDSS J1541, SDSS J1705 and SDSS J2302). Therefore, it is necessary to use the multi-band photometric observations for deriving the orbital periods of short period PCEBs.

The upper limits were estimated for 8 short period PCEBs based on several RV measurements by Morgan et al. (2012), and thus they are hardly considered as their orbital periods. The orbital periods derived for them (except for SDSS J2208) in this work are shorter than the upper limits listed in Morgan et al. (2012), and thus the orbital periods obtained in this work based on the photometric data from ZTF DR19 might be correct. In addition, an orbital period of SDSS

J2302 (with  $P_{\text{orb}} = 0.9098531$  days, Ivezić et al. 2007) is derived to be 0.2376198 days and this object is found to be an eclipsing PCEB in this work. The difference between our result and theirs might be caused by the different observations used. The result obtained for this object by Ivezić et al. (2007) only based on a limited number of repeated observations ( $\sim 10$ , Ivezić et al. 2007). Although a limited number of high-precision observations can reveal the variability of stellar luminosity, it is difficult to obtain their exact periods, so that an eclipsing binary with a much shorter eclipse duration than its orbital period could easily escape detection (Ivezić et al. 2007).

As seen from Fig. 2 and Fig. 9, their optical spectra from LAMOST and/or SDSS show the evident emission line(s) at Balmer series or even He I  $\lambda\lambda 5876$  and  $\lambda\lambda 6681$ . A possible explanation for this behavior is photoionization and recombination due to irradiation of M dwarfs because of their very hot WD companions with an effective temperature higher than  $\sim 10,000$  K (Silvestri et al. 2006). Another one is that the emission features might be a result of the magnetic activity of M dwarf components in these PCEBs, since the M dwarfs in PCEBs are younger, and thus more active than the field M dwarfs (Rebassa-Mansergas et al. 2013b). Therefore, the reflection effect or star spot due to stellar magnetic activity can provide the favorable opportunity for searching the short-period PCEBs from WDMS binaries with emission lines. Meanwhile, the optical spectra of SDSS J0950 and SDSS J1317 show the characteristic spectra ( $\lambda\lambda 8183.27$  and  $\lambda\lambda 8194.81$  absorption doublet) of the M-type dwarfs, suggesting that SDSS J0950 and J1317 should contain an M-type dwarf component. In addition, the emission lines presented in their optical spectra exhibit a single peak, therefore the emission lines in their optical spectra might not be a result of the accretion disk, implying that they are probably not the cataclysmic variables. In fact, the M-type dwarfs in these two PCEBs with an orbital period longer than 1 days cannot fill their Roche lobes to transfer mass to their WD companion and thus form an accretion disk around these white dwarfs, unless the WDs in them are extremely massive ones.

In addition, we have analyzed the SED of SDSS J1541 because of the lack of properties of its cool companion. As a result, it is found that the hot WD SDSS J1541 might be accompanied by a late-type M dwarf, it should be produced by common envelope evolution, however, it is still worth further studies how can its thick common envelope be ejected by a very low orbital energy of the initial binary,

because the WD in it is a He-WD with  $M \lesssim 0.45M_{\odot}$ , suggesting that most of mass of its MS progenitor had been ejected by CE evolution, since the oldest globular clusters in the galactic halo are producing  $\sim 0.53M_{\odot}$  WDs for MS progenitors with  $M \lesssim 0.8M_{\odot}$  (Kalirai et al. 2009; Brown et al. 2011). Meanwhile, it is found in Fig. 6 that the light curves of three PCEBs (SDSS J0747, SDSS J0908 and SDSS J2302) show the evident eclipses, implying that these PCEBs are close eclipsing binaries with a short period. The eclipsing PCEBs can provide us with the possibility to directly obtain their precise parameters independently of atmospheric parameters. Therefore, we would observe these eclipsing PCEBs and analyze their light curves and radial velocity curves to obtain the precise physical parameters for them in the future since their precise parameters are useful to constraint the CE evolution.

## ACKNOWLEDGEMENTS

The authors are grateful to the anonymous referee for the valuable suggestions and insightful remarks, which have improved this work greatly. We also thank prof. D. Koester and P. Bergeron for providing their WD models. This project was partly supported by the Chinese Natural Science Foundations (Nos. 11773065, 11973081 and 12073070), and by the Science Research Grants from National Key R&D Program of China (2021TYFA1600403) and the International Centre of Supernova, Yunnan Key Laboratory (No. 202302AN360001).

Funding for the SDSS and SDSS II provided by the Alfred P. Sloan Foundation, the participating Institutions, the National Science Foundation. The US Department of Energy, the National Aeronautics and Space Administration, the Japanese Monbukagakusho and the Max Plank Society, and the Higher Education Funding Council for England.

This paper makes use of data products of WISE, which is a joint project of the University of California, Los Angeles, and the Jet Propulsion Laboratory/California Institute of Technology, funded by the National Aeronautics and Space Administration. this research has made use of the SIMBAD database VizieR service.

## DATA AVAILABILITY

The data underlying this work will be shared on reasonable requisition to the corresponding author. The various sky survey data can be available in the public Data Release of ZTF DR19.

## REFERENCES

- Abazajian K.N., Adelmann-McCarthy J.K., Agüeros M.A., Allam S.S., et al., 2009, *ApJS*, 182, 543
- Abbott B.P., et al., 2016, *ApJ*, 818, L22
- Anguiano B., Rebassa-Mansergas A., García-Berro E., et al., 2017, *MNRAS*, 469, 2102
- Baraffe I., Chabrier G., Barrman T.S., et al., 2003, *A&A*, 402, 701
- Bédard A., Bergeron P., Brassard P., Fontaine G., 2020, *ApJ*, 901, 93
- Bell R.A., Gustafsson B., 1989, *MNRAS*, 236, 653
- Bergeron P., Wesemel F., Beauchamp A., 1995, *PASP*, 107, 1047
- Brown J.M., Kilic M., Brown W.R., Kenyon S.J., 2011, *ApJ*, 730, 67
- Brown A.J., Parsons S.G., Littlefair S.P. et al., 2022, *MNRAS*, 513, 3050
- Chambers K.C., Magnier E.A., Metcalfe N.N., et al., 2016, arXiv: 1612.05560
- Chen X.D., Wang S., Deng L.C., et al., 2020, *ApJS*, 249, 18
- Davis P.J., Kolb U., Willems B., Gänsicke B.T., 2008, *MNRAS*, 389, 1563
- Debes J.H., Hoard D.W., Wachter S., et al., 2011, *ApJS*, 197, 38
- Dietz S.E., Yoon J.M., Beers T.C., 2020, *ApJ*, 894, 34
- Drake A.J., Djorgovski S.G., García-Álvarez D., et al., 2014, *ApJ*, 790, 157
- Elsenstein D.J., Liebert J., Harris H.C., et al., 2006, *ApJS*, 167, 40
- Farihi J., Hoard D.W., Wachter S., 2006, *ApJ*, 646, 480
- Farihi J., Parsons S.G., Gänsicke B.T., 2017, *Nature Astronomy*, 1, 32
- Gaia Collaboration, Brown A.G., et al., 2021, *A&A*, 649, A1
- Gavras P., Rimoldini L., et al., 2023, *A&A*, 674, A22
- Gentile Fusillo N.P., Gänsicke B.T., & Greiss S., 2015, *MNRAS*, 448, 2260
- Gianninas A., Bergeron P., Ruiz M.T., 2011, *ApJ*, 743, 138
- Gil-Pons P., García-Berro E., 2001, *A&A*, 375, 87
- Girven J., Gänsicke B.T., Steeghs D., Koester D., 2011, *MNRAS*, 417, 1210
- Graham M.J., Kulkarni S.R., Bellm E.C., et al., 2019, *PASP*, 131, 078001
- Green R.F., Schmidt M., Liebert J., 1986, *ApJS*, 61, 305
- Guo J.C., Zhao J.K., Tziamtzis A. et al., 2015, *MNRAS*, 454, 2787
- Han Z.W., Podsiadlowski P., Maxted P.F.L., et al., 2002, *MNRAS*, 336, 449
- Heber U., 1986, *A&A*, 155, 33
- Heinze A.N., Torry J.L., Denneau L., et al., 2018, *AJ*, 156, 241
- Heller R., Homeier D., Dreizler S., Østense R., 2009, *A&A*, 496, 191
- Hjellming M.S., Taam R.E., 1991, *ApJ*, 370, 709
- Holl B., Faricius C., Portell J., et al., 2023, *A&A*, 674, A25
- Iben I.J., Livio M., 1993, *PASP*, 105, 1373
- Ivezić Z., Smith J.A., Miknaitis G., et al., 2007, *AJ*, 134, 973
- Justham S., Wolf C., et al., 2009, *A&A*, 493, 1081
- Kalirai J.S., Davis D.S., Richer H.B., Bergeron P. et al., 2009, *ApJ*, 705, 408
- Kao W., Kaplan D.L., Prince T.A., Tang S.M., Ene I., Kim K.B., et al., 2016, *MNRAS*, 461, 2747
- Kepler S.O., Pelisoli I., Koester D., Ourique G., et al., 2015, *MNRAS*, 446, 4078
- Kepler S.O., Pellisoli I., Koester D., et al., 2019, *MNRAS*, 486, 2169
- Kilic M., Stanek K.Z., Pinsonneault M.H., 2007, *ApJ*, 671, 761
- Kleinman S.J., et al., 2004, *ApJ*, 607, 426
- Kleinman S.J., Kepler S.O., Koester D., et al., 2013, *ApJS*, 204, 5
- Koester D., 2010, *Mem. Soc. Astron. Italiana*, 81, 921
- Lei Z.X., et al., 2013, *A&A*, 549, A145
- Lenz P., Breger M., 2005, *CoAst.*, 146, 53
- Limoges M.M., Bergeron P., 2010, *ApJ*, 714, 1037
- Li L.F., Zhang F.H., Han Q.W., Kong X.Y., Gong X.B., 2014, *MNRAS*, 455, 1331
- Liu C., Li L.F., Zhang F.H., Zhang Y., Jiang D.K., Liu J.Z., 2012, *MNRAS*, 424, 1841
- Luhman K.L., Burgasser A.J., Bochanski J.J., 2011, *ApJ*, 730, L9
- Marsh T.R., Dhillon V.S., Duck S.R., 1995, *MNRAS*, 275, 828
- Masci F.J., Laher R.R., Rusholme B., et al., 2019, *PASP*, 131, 018003
- Miller A.A., 2015, *ApJ*, 811, 30
- Morgan D.P., West A.A., Garcés A., et al., 2012, *AJ*, 144, 93
- Nebot Gómez-Morán A., Schwöpe A.D., Schreiber M.R., et al., 2009, *A&A*, 495, 561
- Nebot Gómez-Morán A., Gänsicke B.T., Schreiber M.R., Rebassa-Mansergas A., et al., 2011, *A&A*, 536, 43
- Nelemans G., Tauris T.M., 1998, *A&A*, 335, L85
- Nordhaus J., 2011, *Int. J. Mod. Phys. E*, 20, 29
- Oswalt T.D., Peterson B.M., Foltz C.B., 1984, *AJ*, 89, 421
- Paczyński B., 1976, in Eggleton P., Mitton S., Whelan J., eds, *Proc. IAU Symp. 73, Structure and Evolution of Close Binary Systems*, Reidel, Dordrecht
- Parsons S.G., Agurto-Gangas C., Gänsicke B.T., et al., 2015, *MNRAS*, 449, 2194
- Parsons S.G., Gänsicke B.T., Marsh T.R., Drake A.J., Dhillon V.S., et al., 2013, *MNRAS*, 429, 256
- Parsons S.G., Hermes J.J., Marsh T.R., et al., 2017, *MNRAS*, 471, 976
- Parsons S.G., Gänsicke B.T., Schreiber M.R., et al., 2021, *MNRAS*, 502, 4305
- Pesch P., Sanduleak N.N., 1983, *ApJS*, 51, 171
- Politano M., Weiler K.P., 2007, *ApJ*, 665, 663
- Politano M., van der Sluis M., Taam R.E., Willems B., 2010, *ApJ*, 720, 1752
- Pourbaix D., Kapp G.R., Szkody P., et al., 2005, *A&A*, 444, 643
- Pyrzas S., Gänsicke B.T., Marsh T.R., et al., 2009, *MNRAS*, 394, 978



- Rappaport S., Vanderburg A., Nelson L., Gary B.L., Kaye T.G., Kalomeni B., et al., 2017, *MNRAS*, 471, 948
- Ritter H., Kollb U., 2003, *A&A*, 404, 301
- Raymond S.N., Szkody P., Hawley S.L., et al., 2003, *AJ*, 125, 2621
- Rebassa-Mansergas A., Gänsicke B.T., Rodríguez-Gil P., et al., 2007, *MNRAS*, 382, 1377
- Rebassa-Mansergas A., Gänsicke B.T., Schreiber M.R., et al., 2008, *MNRAS*, 390, 1635
- Rebassa-Mansergas A., Gänsicke B.T., Schreiber M.R., et al., 2010, *MNRAS*, 402, 620
- Rebassa-Mansergas A., Nebot-Gómez-Morán A., Schreiber M.R., et al., 2011, *MNRAS*, 413, 1121
- Rebassa-Mansergas A., Nebot Gómez-Morán A., Schreiber M.R., Gänsicke B.T., et al., 2012, *MNRAS*, 419, 806
- Rebassa-Mansergas A., Agurto-Gangas C., Schreiber M.R., et al., 2013a, *MNRAS*, 433, 3398
- Rebassa-Mansergas A., Schreiber M.R., Gänsicke B.T., et al., 2013b, *MNRAS*, 429, 3570
- Rebassa-Mansergas A., Solano E., Jiménez-Esteban F.M., 2021, *MNRAS*, 506, 4201
- Rebassa-Mansergas A., Maldonado J., Raddi R., et al., 2023, *MNRAS*, 526, 4787
- Ren J.J., Luo A.L., Li Y.B., Wei P., et al., 2013, *AJ*, 146, 82
- Ren J.J., Rebassa-Mansergas A., Luo A.L., et al., 2014, *A&A*, 570, A107
- Ren J.J., Rebassa-Mansergas A., Parsons S.G., et al., 2018, *MNRAS*, 477, 4641
- Sánchez-Sáez P., Arredondo J., Bayo A., et al., 2023, *A&A*, 675, A195
- Schreiber M.R., Gänsicke B.T., 2003, *A&A*, 406, 305
- Schreiber M.R., Gänsicke B.T., Southworth J., et al., 2008, *A&A*, 484, 441
- Schreiber M.R., Gänsicke B.T., Rebassa-Mansergas A., et al., 2010, *A&A*, 513, L7
- Sesar B., Hernitschek N., Mitrović S., et al., 2017, *AJ*, 153, 204
- Silvestri N.M., Hawley S.L., West A.A., Szkody P., Bochanski J.J., Eisenstein D.J., et al., 2006, *AJ*, 131, 1674
- Silvestri N.M., Lemagie M.P., Hawley S.L., et al., 2007, *AJ*, 134, 741
- Skiff B.A., 2009, *VizieR Online Data Catalog*, 1, 2023
- Taam R.E., Sandquist E.L., 2000, *ARA&A*, 38, 113
- Tonnry J.L., Denneau L., Flewelling H., et al., 2018, *ApJ*, 867, 105
- Tremblay P.E., Bergeron P., Gianninas A., 2011, *ApJ*, 730, 128
- Tremblay P.E., Cukanovaite E., Gentile-Fusilo N.P., et al., 2019, *MNRAS*, 482, 5222
- Tsantaki M., Pancino E., Marrese P. et al., 2022, *A&A*, 659, A95
- van den Besselaar E.J.M., Greimel R., Morales-Rueda L., et al., 2007, *A&A*, 466, 1031
- Verberne S., Koposov S.E., Rossi E.M., et al., *A&A*, 684, A29
- Wagner R.M., Sienn E.M., Liebert J., et al., 1988, *ApJ*, 328, 213
- Webbink R.F., 1984, *ApJ*, 277, 355
- Webbink R.F., 2008, in *Astrophys. Space Sci., Lib.*, 352, ed. E.F. Milone, D.A. Leahy & D.W. Hobill, 233
- Wegner G., McMahan R.K., Boley F., 1987, *AJ*, 94, 1271
- Wegner G., Swanson S.R., 1990, *AJ*, 100, 1274
- West A.A., Hawley S.L., et al., 2008, *AJ*, 135, 785
- Willems B., Kolb B., 2004, *A&A*, 419, 1057
- Wright E.L., et al., 2010, *AJ*, 140, 1868
- Xu S.Y., Jura M., Pantoja B., Klein B., et al., *ApJ*, 806, L5
- York D.G., Adelman J., Anderson J.E.Jr., Anderson S.F., Annis J., et al., 2000, *AJ*, 120, 1579
- Zhang Y.J., Hou W., Luo A.L., et al., 2022, *ApJS*, 259, 38

This paper has been typeset from a  $\text{\TeX}/\text{\LaTeX}$  file prepared by the author.